PCLR: PROGRESSIVELY COMPRESSED LORA FOR MULTIMODAL CONTINUAL INSTRUCTION TUNING

Weicheng Meng[1,2], **Jingyang Qiao**[2,3], **Shaohui Liu**[1,2†], **Zhizhong Zhang**[3,4†], **Yuan Xie**[2,3‡]
[1]Harbin Institute of Technology, Harbin, China
[2]Shanghai Innovation Institute, Shanghal, China
[3]East China Normal University, Shanghal, China
[4]Shanghai Key Laboratory of Computer Software Evaluating and Testing, Shanghai, China
24b903022@stu.hit.edu.cn, 52275901010@stu.ecnu.edu.cn, zzzhang@cs.ecnu.edu.cn,
shliu@hit.edu.cn, yxie@cs.ecnu.edu.cn

ABSTRACT

Continual Instruction Tuning (CIT) enables Large Multimodal Models (LMMs) to rapidly adapt to new tasks without retraining, but it suffers from the catastrophic forgetting problem. By adding new branches, model extension provides a great idea to accommodate novel knowledge while causing huge memory consumption. To jointly address forgetting and memory explosion, we propose the Compression–Integration–Learning (CIL) pipeline, which draws on the memory consolidation processes during human sleep. Compression streamlines old parameters to release capacity. Integration merges knowledge from similar tasks to restore the performance loss due to compression. For example, based on LLaVA-7B, the forgetting is reduced from 11.29 to 5.09. Learning reallocates released capacity for new task-relevant parameters. Next, based on the characteristics of LMMs at different learning stages, we establish the progressive learning process, further reducing forgetting from 5.09 to 3.39. Moreover, to adapt this process, we decompose LoRA into a set of rank vectors and introduce an extremely fine-grained architecture, LoRA Rank Pool (LRP), with the goal of flexible knowledge employment and editing. Finally, we combine all components, and yield **P**rogressively **C**ompressed **Lo**ra (PCLR). Extensive experiments demonstrate that PCLR owns a memory budget close to non-extension methods while outperforming extension methods in performance. The implementation code is available at `https://github.com/SII-HITclearlove777/PCLR`.

1 INTRODUCTION

Large Multimodal Models (LMMs) have gained widespread adoption due to their exceptional cross-modal comprehension and generation capabilities (Lu et al., 2024; Zheng et al., 2023). The training process follows a two-stage paradigm: Pre-Training (PT) and Supervised Fine-Tuning (SFT) (Bai et al., 2025; Chen et al., 2024c). Within SFT, instruction tuning markedly improves the ability of models to follow human intent and become an industry standard practice (Dai et al., 2023; Achiam et al., 2023). However, with continuously evolving data sources and task requirements, the need for frequent retraining is costly and impractical (Scialom et al., 2022; Luo et al., 2023). Thus, Continual Instruction Tuning (CIT) becomes a promising way to learn evolving knowledge for LMMs (Chen et al., 2024a; Xie et al., 2025).

CIT methods include static-structure (non-extension) and model extension (extension) (Yu et al., 2024a). Static methods alleviate forgetting by constraining parameter updates, but they suffer from the trade-off between stability and plasticity (Li & Hoiem, 2017; Aljundi et al., 2018; Zhu et al., 2024). Extension methods append task-specific modules to isolate interference (Wang et al., 2022a; Yu et al., 2024b), but this incurs unbounded memory with tasks growing.

[1]†Corresponding Authors
[2]‡Project Leader

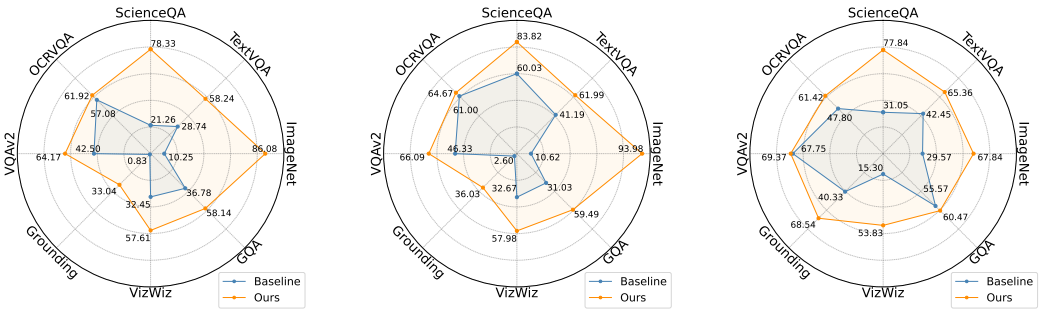

(a) Comparison on LLaVA-7B (b) Comparison on LLaVA-13B (c) Comparison on Qwen-VL

Figure 1: Radar chart of comparisons on Final Accuracy between baseline (LoRA) and ours.

To mitigate memory growth, recent methods focus on conditional extension, assuming task interference correlates with feature distribution differences. Before training, feature distribution similarities between previous tasks and the new task are measured. If no similar previous tasks, an independent parameter group is instantiated to avoid interference; otherwise, the task is assigned to the cluster whose feature distribution is closest to the new task and the corresponding parameter group is trained within a regularization constrained update scheme (He et al., 2023; Qiao et al., 2025a). With treating parameter groups as routing experts, these frameworks mitigate high-interference tasks and reduce the need for extension. Nevertheless, they only implicitly postpone structural extension, and memory will still undergo unbounded growth with a long sequence of tasks.

The memory overhead of the model extension is in fact unnecessary. During continual learning, the LoRA parameters from distinct tasks contain linearly dependent rank vectors (as shown in Figure 2), and these rank vectors are compressible. However, current extension methods ignore fine-grained rank-level relationships, which constitute the key driver of memory explosion. To address the problem, we develop a fine-grained Mixture-of-Experts structure, LoRA Rank Pool (LRP), which is inspired by AdaLoRA (Zhang et al., 2023) and L2P series (Wang et al., 2022c;b; Smith et al., 2023b) (Appendix M). LRP decomposes LoRA into rank experts, providing maximal flexibility for knowledge employment and editing. This design reduces storage overhead by minimizing parameter extension during training and pruning parameters post-training.

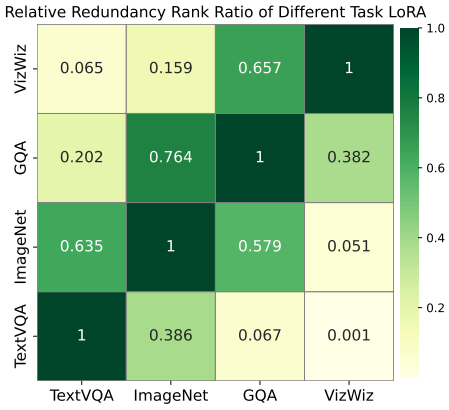

Figure 2: From TextVQA to VizWiz, $\langle \text{VizWiz}, \text{GQA} \rangle$ represents 38.2% ranks in VizWiz's LoRA are redundant versus GQA. Details are shown in Appendix N.

To save memory, we introduce **Compression** after extension: pruning redundant rank experts in LRP to release capacity. Inspired by hippocampal reactivation during sleep that consolidates memory (Wilson & McNaughton, 1994; Stickgold, 2005; Srinivasan et al., 2025), we propose off-learning-phase **Integration**: using knowledge distillation to reactivate learned experts and fuse their internal knowledge, thereby mitigating the performance degradation induced by compression. Combined with **Learning** on new tasks, this yields the **Compression-Integration-Learning (CIL)** pipeline. The memory saved by compression is set equal to that added by learning, aiming to fundamentally eliminate the issue of unbounded extension. Finally, we establish the progressive learning process, effectively mitigating catastrophic forgetting in long-term CIT. Different from previous work, our approach allows all experts to contribute to new task learning, which promotes knowledge transfer and integration. In our method, task-specific experts that support a single task are progressively transformed into mixture-of-experts that support multiple tasks, during continual learning. The evolution is visualized in Appendix F.

We evaluate the proposed method on LLaVA-1.5 (Liu et al., 2024) and Qwen-VL (Bai et al., 2023b) by using the Continual Instruction Tuning benchmark (Chen et al., 2024a). Furthermore, we extend our evaluation to a long-term multimodal CIT benchmark, Continual-NExT. Experimental results demonstrate that PCLR significantly enhances the continual learning capabilities of LMMs. In summary, the contributions of this work are as follows:

- We develop the Compression–Integration–Learning (CIL) pipeline to balance stability, plasticity, and memory efficiency in CIT. Additionally, it can be combined with other regularization strategies to further improve the long-term CIT performance.
- We propose an extremely fine-grained Mixture-of-Experts (MoE) structure, LoRA Rank Pool (LRP), enabling maximal freedom to employ and edit knowledge.
- To the best of our knowledge, PCLR achieves state-of-the-art performance with significant baseline improvements (as shown in Figure 1). In addition, it also owns the superior performance on Continual-NExT (15 tasks), the longest known multimodal CIT benchmark.

2 Related Work

Large Multimodal Models: Benefiting from the advanced understanding and generation capabilities of LLMs (Bai et al., 2023a; Touvron et al., 2023b; Dubey et al., 2024), LMMs achieve rapid development (Zhan et al., 2024; Wang et al., 2024; Team, 2024; Ge et al., 2024), particularly in Visual Large Language Models (VLLMs) (Chen et al., 2024b; Bai et al., 2025; Li et al., 2024a). VLLMs employ linear projection layers (Touvron et al., 2023a; Bai et al., 2023a) and Q-Former (Liu et al., 2023; Zhu et al., 2023) as cross-modal bridge modules to connect visual encoders to LLM backbones (Touvron et al., 2023a; Bai et al., 2023a), enhancing multimodal reasoning.

Multimodal Continual Instruction Tuning: CIT methods can be categorized into three paradigms. Regularization methods constrain gradients or parameters during training (Smith et al., 2023a; Zhu et al., 2024). Structure-based methods enhance performance through architectural modification and dynamic extension (Yan et al., 2021; Jha et al., 2024; Yu et al., 2024b). Replay methods mitigate catastrophic forgetting by replaying high-quality historical samples (Chaudhry et al., 2018; 2019; Yoon et al., 2021; Zhang et al., 2024). To support multimodal CIT research, the CoIN (Chen et al., 2024a) benchmark is introduced. Representative methods: Model Tailor (Zhu et al., 2024) updates critical parameters via sparse masking. Eproj (He et al., 2023) and LCIA (Qiao et al., 2025a) implement grouped parameter learning based on task similarity. Specifically, Eproj introduces similarity-driven dynamic regularization, while LCIA incorporates the dynamic exponential moving average.

3 Preliminary

Problem Definition: Given the LMM M, a series of tasks $T = \{T_1, T_2, \cdots, T_n\}$ and the corresponding instruction datasets $D = \{D_1, D_2, \cdots, D_n\}$, multimodal continual instruction tuning refers to sequentially training M on each new task T_t ($1 \leq t \leq n$) with access only to D_t (or limited access to previous datasets), where $D_t = \{V_i^t, M_i^t, I_i^t\}_{i=1}^{n_t}$, n_t denotes the size of the training set for the t-th task, and V_i^t, M_i^t, I_i^t denote the visual inputs, the textual messages, and the instruction for sample i, respectively. The objective is to acquire new knowledge while preserving performance on previous tasks during continual learning.

LoRA Tuning: LoRA directly interacts with the frozen weights of the original model and has strong performance on complex tasks (Hu et al., 2022). It uses matrix factorisation $\Delta W = \beta AB^T$ to represent weight updates during fine-tuning, where β is a scaling factor, $\Delta W \in \mathbb{R}^{d_{in} \times d_{out}}$, $A \in \mathbb{R}^{d_{in} \times r}$, $B \in \mathbb{R}^{d_{out} \times r}$, and d_{in}, d_{out}, r represent the input dimension, output dimension, and latent dimension, respectively. The forward process is defined as: $y = xW + \beta xAB^T$.

MoE for CIT: The Mixture-of-Experts (MoE) architecture inherently excels in multi-task learning due to its sparse activation mechanism (Guo et al., 2025). Recent methods leverage data features as queries for sequence-level routing: Eproj (He et al., 2023) encodes visual-textual features to assign the task-specific routing expert, while LCIA (Qiao et al., 2025a) identifies instruction patterns to allocate experts. The general formulation can be shown as:

$$y = xW + \beta \sum_{i=1}^{t} gate(s(x), k)_i xA_iB_i^T, \tag{1}$$

where $s(x) \in \mathbb{R}^t$ denotes the expert routing scores, t is the number of total experts, k is the number of activated experts, and A_i, B_i are the LoRA weights of the i-th expert. The operator $gate(v, k)$ selects the top-k entries of vector v, setting those positions to 1 and others to 0. Moreover, to

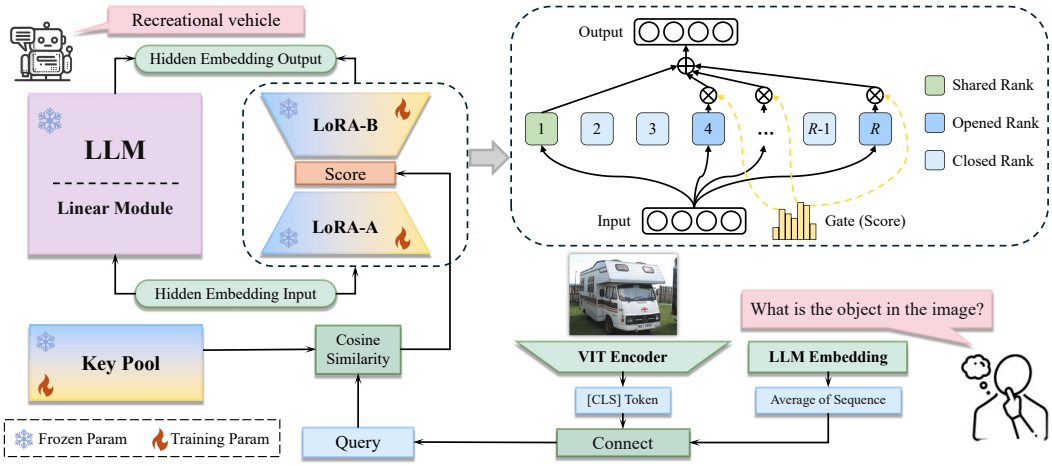

Figure 3: The pipeline of LRP. First, extract the query from inputs. Next, compute similarity scores with the key pools and gate the scores. Then, apply scores jointly with LRP weights in the forward pass. LRP is semi-frozen during training: new parameters are trained while previous ones are frozen.

accommodate continuously growing knowledge, the MoE can be extended by adding new experts, and we refer to this as Dynamic MoE in this paper.

4 METHOD

4.1 OVERVIEW

Our method comprises two coupled components: the LoRA Rank Pool (LRP) architecture and the Compression–Integration–Learning (CIL) pipeline. LRP factorizes LoRA adapters into rank vectors, each paired with a learnable key, forming an atomic expert that is inserted into linear layers. LRP is similar to Dynamic MoE, which uses static features to activate experts and preserves past knowledge during training by freezing parameters (as shown in Figure 3). For the learning paradigm, we design CIL to emulate the memory cycle of human lifelong learning (as shown in Figure 4). Compression, prunes experts at a preset retention rate to release capacity. Integration, applies an improved distillation algorithm to align the post-compression LRP with its original state, thereby compensating for compression-induced loss by merging similar experts. Learning, trains new experts with the released capacity, and initializes them with similar previous experts to enhance forward transfer. Finally, we build a progressive synergy mechanism combining the CIL pipeline and the CIT process to enhance long-term CIT performance (the algorithm is shown in Appendix U.1).

4.2 LORA RANK POOL

Although Dynamic MoE achieves outstanding performance on CIT, its experts tend to acquire overlapping (redundant) knowledge. To address this problem, we decompose experts to the atomic by splitting the LoRA weight A into a column vector set $\{a_1, a_2, \cdots, a_n\}$, and the weight B^T into a row vector set $\{b_1^T, b_2^T, \cdots, b_n^T\}$. Then, we introduce globally shared components A_s, B_s to accumulate global knowledge. Thus, we obtain the LoRA Rank Pool formulation from Eq.(1):

$$y = xW + \beta_s x A_s B_s^T + \beta_m \sum_{i=1}^{n} gate(s(x), r)_i x a_i b_i^T, \tag{2}$$

where n is the number of total rank experts, r is the number of activated rank experts, β_s is the factor of the shared ranks part, β_m is the factor of the mixture-of-experts part.

Next, we define the score function $s(x) = Kq$, where $K \in \mathbb{R}^{n \times d}, q \in \mathbb{R}^d$ are the L2-regularized key pool and query. For each input x, we construct q (query) by concatenating the mean-pooling of text embeddings with the visual output ([CLS] token or mean-pooling). Each rank expert in the LRP is assigned a learnable key, and all keys form K (key pool). We use cosine similarity scores and gating to select top-r relevant experts. This enables the model to employ distinct experts to acquire different knowledge and selectively activate them during inference.

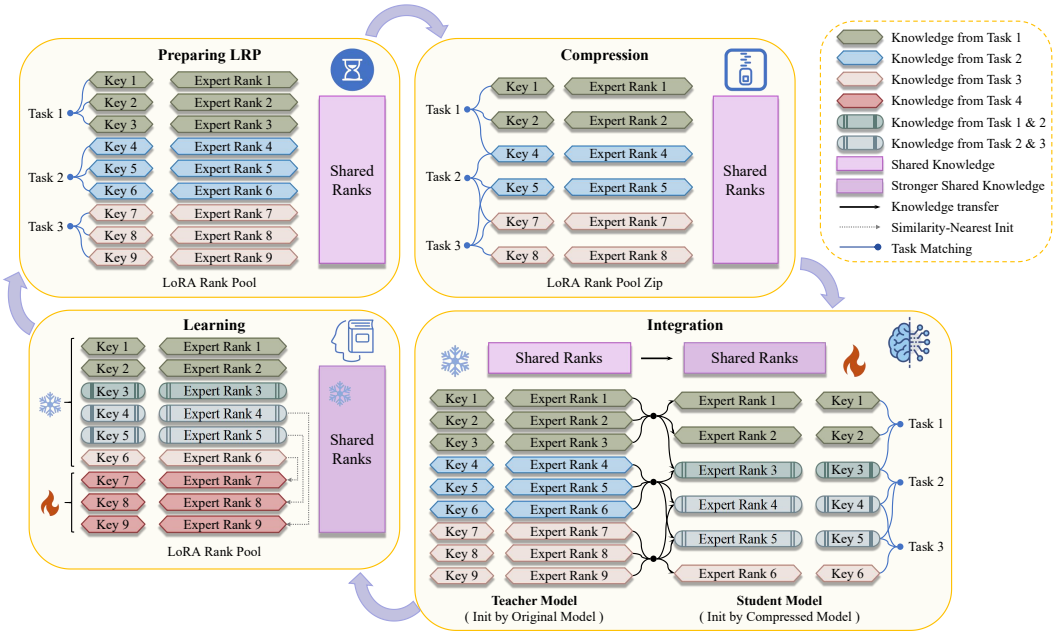

Figure 4: Compression-Integration-Learning (CIL) pipeline. Compression is a training-free process that streamlines the original LRP. Integration is a distillation process that aligns the compressed LRP with the original LRP. Learning is a supervised fine-tuning process that initializes the LRP from the integration-processed LRP and then adapts to the new task.

In Eq.(2), the mixture-of-experts part forms an n-term matrix polynomial. Sequential execution of all terms would cause significant computational overhead, making parallelization necessary. We aggregate the discrete ranks into A_m and B_m. We broadcast the scoring vector $s(x)$ to match the dimensions of xA_m and derive a parallelized formulation:

$$y = xW + \beta_s x A_s B_s^T + \beta_m F\left(xA_m, gate\left(Kq, r\right)^T\right) B_m^T, \tag{3}$$

where the operator $F\left(U, v\right)$ broadcasts $v \in \mathbb{R}^b$ to match the shape of $U \in \mathbb{R}^{a\times b}$, resulting in two matrices with identical dimensions, followed by an element-wise multiplication.

To jointly improve downstream task performance and learn the keys of labeled experts within the LRP, we combine the cross-entropy loss with the query–key cosine similarity loss:

$$\mathcal{L}\left(\theta\right) = -\frac{1}{T}\sum_{t=1}^{T}\log P_\theta\left(y_t \mid x, y_{<t}, q\right) + \frac{\lambda}{l}\sum_{i=1}^{l}\left\|\mathbf{1}_r - top_r(K_i)q\right\|_1, \tag{4}$$

where λ is a balancing hyperparameter, and l denotes the number of key pools, which equals the LMMs layer count. To preserve previous knowledge, we freeze all previous keys and ranks while optimizing only the newly added ones.

4.3 Compression-Integration-Learning

Conventional learning faces the dilemma of whether to learn within the previous parameter space or to allocate a new one. The former suffers from the trade-off between stability and plasticity, whereas the latter leads to unbounded memory growth. To address this problem, we propose the Compression-Integration-Learning (CIL) pipeline, which compresses previous knowledge when learning new tasks. We decompose each CIT task into three main phases: compressing, integrating past knowledge, and learning new knowledge (as shown in Figure 4). Notice that CIL is initiated once the total rank reaches a predefined value.

Compression: At this phase, we introduce a compression retention rate $\alpha \in (0, 1]$, discarding a portion of redundant rank experts and their corresponding keys. As a result, the pruned LRP maintains its rank and key count at α times the values of the original one. Although compression may lead to performance loss, it is crucial for alleviating the memory pressure of the learning system.

Integration: Removing key-value pairs will degrade knowledge from previously learned tasks. To compensate for this loss, we perform integration on the current dataset to adapt the LRP using the distillation loss (Hinton et al., 2015; Huang & Wang, 2017; Gou et al., 2021). Specifically, we formulate the Query-based Kullback-Leibler Divergence Loss (QKLD Loss) to align the compressed LRP with the original one. The process freezes the teacher model (LRP before compression) and updates the student model (LRP after compression). Through distillation, rank experts in LRP absorb the knowledge from pruned experts, and the common representations across different tasks flow into the shared knowledge space, ultimately mitigating the knowledge loss caused by compression. The pseudo algorithm of compression and integration can be referred to in Appendix U.3.

LRP activates specific rank experts based on the query of the input. However, the datasets from previous tasks are not accessible during integration. Considering that we optimize the query–key cosine similarity during learning, and its optimum is achieved when each new key equals the mean of all queries for the corresponding task. Therefore, the learned keys can serve as surrogates for the queries from previous tasks, and we define them as fake queries. During integration, we compute Kullback-Leibler Divergence (KLD) to quantify the performance loss associated with the fake query:

$$D_{KL}\left(q\right)=\frac{1}{T}\sum_{t=1}^{T}P_{\theta_{ori}}\left(x_t\mid x_{<t},q\right)\log\left(\frac{P_{\theta_{ori}}\left(x_t\mid x_{<t},q\right)}{P_{\theta_{zip}}\left(x_t\mid x_{<t},q\right)}\right), \tag{5}$$

where θ_{ori} is the original LRP, θ_{zip} is the compressed LRP, x is the input. To emphasize optimization for tasks with larger performance degradation, we define the sampling probability of fake query:

$$P\left(q\right)=\frac{\sqrt{D_{KL}\left(q\right)}}{\sum_{q\in K_{ori}}\sqrt{D_{KL}\left(q\right)}}, \tag{6}$$

where K_{ori} is the original key pool. Finally, we define the QKLD Loss:

$$\mathcal{L}\left(\theta_{zip}\right)=\mathbb{E}_{q\sim P}[D_{KL}\left(q\right)]=\sum_{q\in K}P(q)D_{KL}\left(q\right). \tag{7}$$

Learning: During the learning phase, shared and previous ranks are frozen to preserve past knowledge, while new key–value pairs (rank experts and their corresponding keys) are trained using the capacity released through compression to optimize the new task. By decomposing LoRA into rank vectors, we enhance forward transfer: new parameters are initialized using ranks from similar tasks. This is achieved by computing the queries of a subset of training samples before learning, taking their mean as an identifier to match to key-value pairs in the LRP, and initializing the new rank components with the values corresponding to the keys that exhibit the top-r cosine similarity scores. The pseudo algorithm of learning can be referred to in Appendix U.2.

4.4 Progressive Learning Process

In this section, we introduce the progressive learning process to further improve the continual learning performance of LMMs. In the early CIT, the rank space has not attained its allotted capacity, rendering compression an unnecessary expense. Thus, we disable compression until the capacity is filled. This optimization reduces training cost and avoids unnecessary performance degradation without altering the final number of rank experts and the model memory.

As the number of tasks increases, LMMs accumulate more knowledge and strengthen their capabilities. This means that when learning new tasks, the number of additional trainable parameters progressively decreases, because much of the relevant knowledge has already been encountered. Consequently, the learning focus shifts from acquiring entirely new knowledge to organizing and consolidating acquired knowledge. In the CIL pipeline, overlap between new tasks and earlier knowledge (reusable knowledge) increases. Meanwhile, internal representation becomes increasingly compact and resistant to further compression (high knowledge density).

Accordingly, in the later CIT, we allocate fewer new ranks and employ a lighter, high-retention compression scheme to minimize performance degradation. This encourages LMMs to rely more on frozen knowledge during the late learning phase and has negligible impact on new task performance. The progressive learning process, through deliberate planning of the learning path for LMMs, further enhances stability, plasticity, memory efficiency, and temporal efficiency of its evolution.

Table 1: Comparisons between ours and baselines on LLaVA-1.5-7B, CoIN benchmark.

Method	Venue	Accuracy on Each Task								Overall Results		
		1-ScienceQA	2-TextVQA	3-ImageNet	4-GQA	5-VizWiz	6-Grounding	7-VQAv2	8-OCRVQA	Avg.ACC(↑)	Forgetting(↓)	New.ACC(↑)
Zero-shot	-	49.91	2.88	0.33	2.08	0.90	0.00	0.68	0.17	7.12	-	-
Multi-Task	-	56.77	49.35	95.55	56.65	53.90	30.09	59.50	55.65	57.18	-	-
LoRA (Hu et al., 2022)	ICLR'22	21.26	28.74	10.25	36.78	32.45	0.83	42.50	57.08	28.74	37.29	61.36
LwF (Li & Hoiem, 2017)	TPAMI'16	63.14	39.60	8.90	34.83	14.53	2.48	40.67	62.35	33.31	22.32	52.58
EWC (Kirkpatrick et al., 2017)	PNAS'17	67.41	40.41	8.18	35.05	37.88	2.67	41.27	61.02	36.74	20.51	54.68
MoELoRA (Chen et al., 2024a)	NIPS'24	58.92	38.59	8.85	37.10	44.25	2.45	41.40	55.35	35.86	25.71	58.36
AdaLoRA (Zhang et al., 2023)	ICLR'23	73.40	51.29	35.47	44.53	46.75	0.93	55.86	62.03	46.28	23.99	63.27
MT (Zhu et al., 2024)	ICML'24	79.63	55.47	35.64	58.70	44.37	32.20	62.21	61.59	53.73	14.03	66.00
PGP (Qiao et al., 2025b)	ICLR'24	85.17	56.85	32.26	61.74	49.43	32.74	65.74	62.20	55.77	12.94	67.09
CIA* (Qiao et al., 2025a)	ICML'25	75.63	54.47	43.64	60.70	43.37	36.00	65.21	63.59	55.33	7.04	61.49
SEFE (Chen et al., 2025)	ICML'25	75.35	58.66	83.10	54.25	48.85	16.75	65.35	66.25	58.57	11.94	69.02
ProgLoRA (Yu et al., 2025)	ACL'25	74.84	51.83	83.90	49.93	53.87	31.19	62.71	64.44	59.09	7.53	65.68
EProj (He et al., 2023)	ArXiv'23	78.51	57.53	92.35	55.93	44.67	36.59	63.74	57.00	60.79	5.42	65.54
PCLR	-	**78.33**	**58.24**	**86.08**	**58.14**	**57.61**	**33.04**	**64.17**	**61.92**	**62.19**	**3.39**	**65.16**

4.5 Integration with Regularization Methods

To further enhance the performance of our proposed PCLR on long-term CIT while minimizing unnecessary performance degradation and training overhead, we integrate it with regularization methods. Specifically, the long sequence of tasks is partitioned into groups of contiguous tasks. Within each group we perform continual learning in a unified rank space combined with regularization methods, while across groups we retain the CIL process, thereby avoiding unnecessary extension and compression. This optimization enhances the long-term CIT performance of PCLR while markedly reducing training overhead. We present cases of the integration of PCLR with LwF (Li & Hoiem, 2017) in the experiments, and the pseudo algorithm can be referred to in Appendix U.4.

5 Experiments

5.1 Experimental Setup

CoIN Benchmark: To verify the performance of our method in challenging scenarios, we adopt LLaVA-1.5 (Liu et al., 2023)/Qwen-VL (Bai et al., 2023b) as the base model, and insert the PCLR module into the linear layers of the LLM backbone network and the cross-modal bridge. We use the CoIN (Chen et al., 2024a) benchmark and keep the order of ScienceQA (Lu et al., 2022), TextVQA (Singh et al., 2019), ImageNet (Russakovsky et al., 2015), GQA (Hudson & Manning, 2019), VizWiz (Gurari et al., 2018), Grounding (Mao et al., 2016), VQAv2 (Goyal et al., 2017), and OCRVQA (Mishra et al., 2019). These visual language datasets encompass a diverse range of task types, including selection, classification, grounding, and open-ended question answering.

Continual-NExT Benchmark: In order to further verify our method in the long-term CIT setting, we use the Continual-NExT (Xie et al., 2025) benchmark, and keep the order of ArXivQA (Li et al., 2024b), GeoChat (Kuckreja et al., 2024), IconQA (Lu et al., 2021), ClevrMath (Lindström & Abraham, 2022), CodeQA (Liu & Wan, 2021), ImageNet (Russakovsky et al., 2015), Flickr30k (Plummer et al., 2015), DocVQA (Mathew et al., 2021), TextVQA (Singh et al., 2019), MathQA (Amini et al., 2019), ChartQA (Masry et al., 2022), PathVQA (He et al., 2020), Grounding (Mao et al., 2016), ScienceQA (Lu et al., 2022), and WikiQA (Yang et al., 2015). These visual language and pure language datasets cover multiple fields such as coding, mathematics, remote sensing and medical images. The experimental setup is shown in Appendix B.

Comparison Methods: Compared baselines include LoRA (Hu et al., 2022), zero-shot and multi-task; regularization methods: (1) LWF (Li & Hoiem, 2017), (2) EWC (Kirkpatrick et al., 2017), (3) GEM (Lopez-Paz & Ranzato, 2017), (4) MT (Zhu et al., 2024), (5) PGP (Qiao et al., 2025b), (6) CIA* (w/o Instruction Grouping) (Qiao et al., 2025a), (7) SEFE (Chen et al., 2025); static-structure method: (1) MoELoRA (Chen et al., 2024a), (2) AdaLoRA (Zhang et al., 2023); extension methods: (1) Eproj (He et al., 2023), (2) CIA (Qiao et al., 2025a), (3) ProgLoRA (Yu et al., 2025); replay method: (1) Experience Replay (Rolnick et al., 2019). The experiments all adopt the setting of training each task for 1 epoch. The method details are provided in Appendix S.

Evaluation Metrics: We utilize three popular evaluation metrics: the average accuracy (Avg.ACC), the forgetting (Forgetting) and the new accuracy (New.ACC), which are shown in Appendix E.

5.2 Main Results

As shown in Table 1, we discover that PCLR achieves the highest overall performance on the CoIN benchmark. Compared to the former best regularization method SEFE, the Avg.ACC improves by

Table 2: Comparisons between ours and baselines on LLaVA-1.5-hf, Continual-NExT benchmark.

Method	Venue	Accuracy on Each Task & Overall Results								
		1-ArxivQA	2-GeoChat	3-IconQA	4-ClevrMath	5-CodeQA	6-ImageNet	7-Flickr30k	8-DocVQA	9-TextVQA
Zero-shot	-	36.99	67.67	18.77	20.27	0.26	18.10	17.27	14.58	57.39
Multi-Task	-	64.08	96.40	60.60	70.50	10.81	97.06	20.52	23.18	65.44
LoRA (Hu et al., 2022)	ICLR'22	53.99	92.23	47.23	44.86	4.36	67.84	17.16	16.47	47.70
LwF (Li & Hoiem, 2017)	TPAMI'16	51.04	87.33	30.97	39.20	4.74	84.89	16.26	16.56	54.09
EWC (Kirkpatrick et al., 2017)	PNAS'17	55.16	91.73	47.17	49.30	4.38	82.03	16.71	16.88	51.73
GEM (Lopez-Paz & Ranzato, 2017)	NIPS'17	55.30	91.03	49.13	48.30	4.76	76.20	16.21	15.85	51.33
Replay-100 (Rolnick et al., 2019)	NIPS'19	54.85	94.40	51.73	40.07	4.48	94.61	9.36	14.65	54.70
MoELoRA (Chen et al., 2024a)	NIPS'24	56.00	91.36	48.76	48.90	3.82	82.19	17.77	16.33	59.51
CIA* (Qiao et al., 2025a)	ICML'25	56.35	93.41	48.76	48.20	4.23	83.00	16.54	16.98	51.32
PCLR	-	**59.00**	**78.20**	**51.30**	**37.17**	**7.86**	**85.19**	**18.68**	**20.00**	**64.10**
PCLR-LwF (PCLR variant)	-	**61.16**	**96.37**	**62.40**	**64.70**	**8.68**	**97.46**	**20.63**	**19.84**	**63.97**
		10-MathQA	11-ChartQA	12-PathVQA	13-Grounding	14-ScienceQA	15-WikiQA	Avg.ACC(↑)	Forgetting(↓)	New.ACC(↑)
Zero-shot	-	0.44	9.60	33.29	28.28	66.19	17.54	27.11	-	-
Multi-Task	-	36.01	20.76	58.61	72.03	86.21	23.38	53.71	-	-
LoRA (Hu et al., 2022)	ICLR'22	33.80	18.04	50.98	69.52	89.46	22.27	45.06	11.62	55.91
LwF (Li & Hoiem, 2017)	TPAMI'16	30.05	18.64	52.79	64.11	87.95	24.96	44.24	12.29	55.70
EWC (Kirkpatrick et al., 2017)	PNAS'17	35.41	19.00	50.92	69.92	89.51	24.17	46.93	9.72	56.01
GEM (Lopez-Paz & Ranzato, 2017)	NIPS'17	35.28	17.68	51.38	67.23	89.86	23.85	46.23	10.19	55.74
Replay-100 (Rolnick et al., 2019)	NIPS'19	31.42	14.40	49.64	56.98	85.62	23.85	45.38	11.41	56.03
MoELoRA (Chen et al., 2024a)	NIPS'24	34.17	18.52	49.04	67.65	88.28	22.59	46.99	8.06	54.51
CIA* (Qiao et al., 2025a)	ICML'25	32.56	17.62	50.47	69.86	89.37	23.54	46.81	8.30	54.55
PCLR	-	**36.42**	**20.96**	**58.48**	**69.76**	**89.65**	**22.27**	**47.94**	**7.71**	**55.14**
PCLR-LwF (PCLR variant)	-	**37.22**	**19.84**	**58.42**	**62.83**	**83.09**	**33.49**	**52.67**	**4.58**	**56.89**

3.62 and the Forgetting decreases by 8.55, demonstrating strong continual learning ability. Additionally, some early approaches (e.g., LwF and EWC) tend to overemphasize the mitigation of forgetting, while they suffer from severe plasticity reduction. Recent methods (such as MT and EProj) place greater importance on maintaining plasticity, contributing to significant improvements in New.ACC. However, these methods still struggle to achieve an optimal balance between New.ACC and Forgetting. Notably, our proposed method, PCLR, achieves the highest New.ACC and the lowest Forgetting among all compared approaches, demonstrating its superior performance. Furthermore, PCLR surpasses both the previous best extension method (EProj) and the leading dynamic update method (CIA*). To validate PCLR's stability and scalability on larger models and diverse architectures, we conduct evaluations on LLaVA-1.5-13B and Qwen-VL. Detailed results are provided in Appendix A. Additionally, we present several visualizations in Appendix C.

As shown in Table 2, our method exceeds the best of other methods (MoELoRA), improving Avg.ACC by 0.95 and reducing Forgetting by 0.35, demonstrating that PCLR sustains strong performance on the long-term Continual-NExT benchmark. To further enhance PCLR's efficiency and performance, we merge it with LwF to form PCLR-LwF. Specifically, we group adjacent tasks and perform LwF fine-tuning within each group (details are shown in Appendix B and Appendix K). This integration with a simple baseline yields notable gains over the original PCLR, improving Avg.ACC by 4.73 and reducing Forgetting by 3.13. Additionally, the results of Qwen2.5-VL-Instruct (Bai et al., 2025) are provided in Appendix A. The visualization is shown in Appendix G.

5.3 Robust Experiments

To verify that PCLR exhibits strong robustness under different CIT settings, we conduct two sets of experiments on instruction templates and learning orders. Note that, in double-row tables, the upper row denotes the immediate accuracy (evaluate after the current task), and the lower row denotes the final accuracy (evaluate after the final task).

Table 3: Results of LLaVA-1.5-7B on **different instruction templates**.

Type	Accuracy on Each Task								Overall Results		
	1-ScienceQA	2-TextVQA	3-ImageNet	4-GQA	5-VizWiz	6-Grounding	7-VQAV2	8-OCRVQA	Avg.ACC	Forgetting	New.ACC
Origin	83.47	61.29	96.50	59.97	58.32	34.02	65.75	61.92	62.19	3.39	65.16
	78.33	58.24	86.08	58.14	57.61	33.04	64.17	61.92			
Diverse	83.47	61.36	96.57	60.03	58.53	34.23	65.83	61.96	62.00	3.71	65.25
	76.92	56.46	86.36	57.93	57.54	33.06	65.75	61.96			
10Type	84.58	60.89	96.40	59.59	58.21	34.14	65.67	60.99	61.98	3.52	65.06
	80.24	58.62	84.81	57.85	56.59	32.29	64.44	60.99			

Different Instruction Templates: As part of the text input, different instructions can influence query encoding and current task learning. We select three instruction templates (details are shown in Appendix I) for comparison, as shown in Table 3. We observe that changes in the instructions incur only a negligible effect, and our method can be adapted to different instruction templates.

Different Learning Order: In CIT, interfering tasks suffer from severe catastrophic forgetting when learned in adjacent order without parameter grouping. PCLR smoothly transitions task-specific experts to mixture-of-experts through the CIL pipeline, which can resist this interference phenomenon

Table 4: Results of LLaVA-1.5-7B on **different task orders**.

Order	Accuracy on Each Task								Overall Results		
	1-ScienceQA	2-TextVQA	3-ImageNet	4-GQA	5-VizWiz	6-Grounding	7-VQAV2	8-OCRVQA	Avg.ACC	Forgetting	New.ACC
Origin	83.47	61.29	96.50	59.97	58.32	34.02	65.75	61.92	62.19	3.39	65.16
	78.33	58.24	86.08	58.14	57.61	33.04	64.17	61.92			
	1-OCRVQA	2-VQAV2	3-Grounding	4-VizWiz	5-GQA	6-ImageNet	7-TextVQA	8-ScienceQA	Avg.ACC	Forgetting	New.ACC
Reverse	58.97	65.06	34.40	58.42	61.08	96.61	60.40	83.68	62.18	3.03	64.83
	56.78	62.66	26.68	55.85	57.00	94.02	60.74	83.68			
	1-GQA	2-Grounding	3-ImageNet	4-OCRVQA	5-ScienceQA	6-TextVQA	7-VizWiz	8-VQAV2	Avg.ACC	Forgetting	New.ACC
Alphabet	60.14	33.10	96.69	61.49	83.97	60.52	57.10	64.34	60.62	4.63	64.67
	59.70	27.32	83.88	50.15	82.72	59.94	56.89	64.34			

to a certain extent. In order to verify that PCLR has strong adaptability to different CIT orders, we compare three settings with different task orders. As shown in Table 4, task order changes induce slight knowledge conflicts, and have minor impact on the overall continual learning performance.

5.4 Ablation Study

To evaluate each PCLR component, we start from the LoRA baseline, add components incrementally, and compare continual instruction tuning performance. Results are shown in Table 5. The experimental results demonstrate that each proposed component is effective in enhancing accuracy and reducing forgetting of LMMs. To validate the superiority of the LRP architecture, we compare the LoRA baseline with the LRP (which only performs compression and learning). We can observe that the introduction of the LRP architecture increases Avg.ACC (+25.92) and reduces Forgetting (-26). In addition, we retain LRP and compare the Compression-Integration-Learning (CIL) and Compression-Learning (CL) processes to validate the effectiveness of the integration process, and the results show that integration increases Avg.ACC (+6.12) and reduces Forgetting (-6.2). Moreover, we observe that the introduction of the progressive process further increases Avg.ACC (+1.41) and reduces Forgetting (-1.7). In summary, compared with the baseline, PCLR increases Avg.ACC (+33.45) and New.ACC (+3.8), reduces Forgetting (-33.9), and achieves an optimal balance between plasticity and stability.

Table 5: Ablation study results.

Method	Avg.ACC(↑)	Forgetting(↓)	New.ACC(↑)
LoRA(Baseline)	28.74	37.29	61.36
w/o Integration Process	54.66	11.29	64.54
w/o Progressive Process	60.78	5.09	65.23
PCLR(Ours)	**62.19**	**3.39**	**65.16**

5.5 The Impact of Progressive Learning

To investigate the impact of different compression strategies on CIT, we designed five methods: Aggressive (non-progressive), Conservative (non-progressive), Reverse Progressive, Centralized Compression, and Progressive Compression (Ours). These methods differ only in their compression strategies while maintaining the same memory usage (details are shown in Appendix J).

Table 6: Results of LLaVA-1.5-7B on **different compression strategies**.

Strategy	Final Accuracy on Each Task								Overall Results		
	1-ScienceQA	2-TextVQA	3-ImageNet	4-GQA	5-VizWiz	6-Grounding	7-VQAV2	8-OCRVQA	Avg.ACC	Forgetting	New.ACC
Aggressive	76.02	57.03	82.61	55.84	57.24	30.71	63.86	62.92	60.78	5.09	65.23
Conservative	81.37	59.23	92.28	58.77	54.55	25.88	64.16	59.03	61.91	1.77	63.43
Reverse	79.13	58.79	87.41	58.51	53.39	25.67	64.44	62.76	61.26	3.21	64.07
Centralized	77.72	53.78	88.93	60.05	55.71	28.71	62.93	60.16	61.00	3.38	64.37
Ours	**78.33**	**58.24**	**86.08**	**58.14**	**57.61**	**33.04**	**64.17**	**61.92**	**62.19**	**3.39**	**65.16**

As shown in Table 6, Aggressive Compression improves performance on new tasks but lacks the ability to consolidate old knowledge (stability), with Forgetting increased (+1.7). Conservative Compression reduces forgetting but limits the ability to learn new tasks (plasticity), with New.ACC decreased (-1.73). Reverse Progressive Compression exhibits subpar performance in both stability and plasticity, with Avg.ACC decreased (-0.93). Centralized Compression also demonstrates overall lower performance, with Avg.ACC decreased (-1.19). In contrast, Progressive Compression dynamically adjusts the compression retention rate, outperforming other strategies in reducing forgetting (Forgetting = 3.39) and enhancing new task learning ability (New.ACC = 65.16), achieving the best overall performance (Avg.ACC = 62.19). By optimizing the learning trajectory based on changes in task knowledge density, Progressive Compression strikes a balance between stability and plasticity, providing an effective design solution for our system development.

Table 7: The results of LLaVA-1.5-13B on **different integration data usage**. For the double-row table, the upper row denotes the final accuracy, and the lower row denotes the integration cost.

IDU	Accuracy and Integration Cost on Each Task								Evaluation Metrics		
	1-ScienceQA	2-TextVQA	3-ImageNet	4-GQA	5-VizWiz	6-Grounding	7-VQAV2	8-OCRVQA	Avg.ACC	Forgetting	Avg.ICost
0	81.63 -	60.84 -	56.55 -	55.83 -	52.95 -	34.51 -	67.64 -	65.27 -	59.40	8.86	-
5k	83.49 -	61.33 -	91.09 -	58.11 14 min	54.41 7 min	35.92 12 min	67.47 10 min	64.17 -	64.50	3.11	11 min
10k	83.33 -	61.35 -	93.15 -	58.39 26 min	55.94 13 min	35.76 23 min	67.29 18 min	64.12 -	64.92	2.61	20 min
20k	83.57 -	61.47 -	94.34 -	58.90 49 min	56.82 24 min	34.31 45 min	66.88 35 min	64.82 -	65.14	2.27	38 min
Origin	83.82 -	61.99 -	93.98 -	59.49 173 min	57.98 24 min	36.03 121 min	66.09 141 min	64.67 -	65.51	2.08	115 min

5.6 Efficiency Analysis

All LRP computations are fully parallelizable with the training cost close to the MoELoRA with one expert (Appendix L). For PCLR, the primary additional cost arises from the integration. We control the integration strength by varying the amount of integration data usage. Specifically, Integration Data Usage (IDU) is set to 5 levels: 0, 5k, 10k, 20k samples, and Origin. Here, **0** denotes no integration, and **Origin** refers to the full dataset for the current task. Experiments are conducted on LLaVA-1.5-13B. Results are reported in Table 7 (Avg.ICost denotes the average integration-phase cost in minutes). In this paper, we use the **Origin** level to obtain the best performance.

In conclusion, PCLR does not incur significant time cost, and appropriately reducing the IDU will not cause serious performance degradation. When computing resources are sufficient, the IDU can be increased to pursue the best final performance.

6 Conclusion

In this work, we introduce PCLR, which provides an extremely fine-grained LoRA Rank Pool (LRP) with a Compression–Integration–Learning (CIL) pipeline to balance stability, plasticity, and memory efficiency during CIT. LRP provides maximal flexibility for expert employment and editing. CIL progressively compresses LRP, trading off a minor performance drop to eliminate unlimited model extension. On CoIN and Continual-NExT benchmarks across multiple LMMs, it delivers superior overall performance to former regularization methods while remaining competitive with extension methods. Robustness studies demonstrate the stability of the method. Ablation experiments confirm the necessity of each component. Efficiency analyses guide our selection of the optimal amount of integration data usage, balancing performance and speed. Owing to computing resource limits, we currently focus on image–text CIT. In the future, we aim to extend our method to modality extension scenarios. Additionally, we will design effective spatial structures in a block-wise manner to further improve memory efficiency (feasibility can be found in Appendix D).

Acknowledgments

This work is supported by the National Natural Science Foundation of China (Grant No. 62476090, 62302167, U23A20343, 62502159), Science and Technology Commission of Shanghai Municipality (Grant No. 25511102700), Natural Science Foundation of Shanghai (Grant No. 25ZR1402135), Natural Science Foundation of Chongqing (Grant No. CSTB2023NSCQ-JQX0007, CSTB2025NSCQ-GPX0445), Open Project Program of the State Key Laboratory of CAD&CG (Grant No. A2501), Zhejiang University, Open Research Fund of Key Laboratory of Advanced Theory and Application in Statistics and Data Science-MOE, ECNU.

References

Josh Achiam, Steven Adler, Sandhini Agarwal, Lama Ahmad, Ilge Akkaya, Florencia Leoni Aleman, Diogo Almeida, Janko Altenschmidt, Sam Altman, Shyamal Anadkat, et al. Gpt-4 technical report. *arXiv preprint arXiv:2303.08774*, 2023.

Rahaf Aljundi, Francesca Babiloni, Mohamed Elhoseiny, Marcus Rohrbach, and Tinne Tuytelaars. Memory aware synapses: Learning what (not) to forget. In *Proceedings of the European conference on computer vision (ECCV)*, pp. 139–154, 2018.

Aida Amini, Saadia Gabriel, Peter Lin, Rik Koncel-Kedziorski, Yejin Choi, and Hannaneh Hajishirzi. Mathqa: Towards interpretable math word problem solving with operation-based formalisms. *arXiv preprint arXiv:1905.13319*, 2019.

Jinze Bai, Shuai Bai, Yunfei Chu, Zeyu Cui, Kai Dang, Xiaodong Deng, Yang Fan, Wenbin Ge, Yu Han, Fei Huang, et al. Qwen technical report. *arXiv preprint arXiv:2309.16609*, 2023a.

Jinze Bai, Shuai Bai, Shusheng Yang, Shijie Wang, Sinan Tan, Peng Wang, Junyang Lin, Chang Zhou, and Jingren Zhou. Qwen-vl: A versatile vision-language model for understanding, localization, text reading, and beyond, 2023b. URL https://arxiv.org/abs/2308.12966.

Shuai Bai, Keqin Chen, Xuejing Liu, Jialin Wang, Wenbin Ge, Sibo Song, Kai Dang, Peng Wang, Shijie Wang, Jun Tang, et al. Qwen2. 5-vl technical report. *arXiv preprint arXiv:2502.13923*, 2025.

Arslan Chaudhry, Marc'Aurelio Ranzato, Marcus Rohrbach, and Mohamed Elhoseiny. Efficient lifelong learning with a-gem. *arXiv preprint arXiv:1812.00420*, 2018.

Arslan Chaudhry, Marcus Rohrbach, Mohamed Elhoseiny, Thalaiyasingam Ajanthan, Puneet K Dokania, Philip HS Torr, and Marc'Aurelio Ranzato. On tiny episodic memories in continual learning. *arXiv preprint arXiv:1902.10486*, 2019.

Cheng Chen, Junchen Zhu, Xu Luo, Heng T Shen, Jingkuan Song, and Lianli Gao. Coin: A benchmark of continual instruction tuning for multimodel large language models. *Advances in Neural Information Processing Systems*, 37:57817–57840, 2024a.

Jinpeng Chen, Runmin Cong, Yuzhi Zhao, Hongzheng Yang, Guangneng Hu, Horace Ho Shing Ip, and Sam Kwong. Sefe: Superficial and essential forgetting eliminator for multimodal continual instruction tuning, 2025. URL https://arxiv.org/abs/2505.02486.

Zhe Chen, Weiyun Wang, Yue Cao, Yangzhou Liu, Zhangwei Gao, Erfei Cui, Jinguo Zhu, Shenglong Ye, Hao Tian, Zhaoyang Liu, et al. Expanding performance boundaries of open-source multimodal models with model, data, and test-time scaling. *arXiv preprint arXiv:2412.05271*, 2024b.

Zhe Chen, Jiannan Wu, Wenhai Wang, Weijie Su, Guo Chen, Sen Xing, Muyan Zhong, Qinglong Zhang, Xizhou Zhu, Lewei Lu, et al. Internvl: Scaling up vision foundation models and aligning for generic visual-linguistic tasks. In *Proceedings of the IEEE/CVF conference on computer vision and pattern recognition*, pp. 24185–24198, 2024c.

Wei-Lin Chiang, Zhuohan Li, Ziqing Lin, Ying Sheng, Zhanghao Wu, Hao Zhang, Lianmin Zheng, Siyuan Zhuang, Yonghao Zhuang, Joseph E Gonzalez, et al. Vicuna: An open-source chatbot impressing gpt-4 with 90%* chatgpt quality. *See https://vicuna. lmsys. org (accessed 14 April 2023)*, 2(3):6, 2023.

Wenliang Dai, Junnan Li, Dongxu Li, Anthony Tiong, Junqi Zhao, Weisheng Wang, Boyang Li, Pascale N Fung, and Steven Hoi. Instructblip: Towards general-purpose vision-language models with instruction tuning. *Advances in neural information processing systems*, 36:49250–49267, 2023.

Abhimanyu Dubey, Abhinav Jauhri, Abhinav Pandey, Abhishek Kadian, Ahmad Al-Dahle, Aiesha Letman, Akhil Mathur, Alan Schelten, Amy Yang, Angela Fan, et al. The llama 3 herd of models. *arXiv e-prints*, pp. arXiv–2407, 2024.

Yuying Ge, Sijie Zhao, Jinguo Zhu, Yixiao Ge, Kun Yi, Lin Song, Chen Li, Xiaohan Ding, and Ying Shan. Seed-x: Multimodal models with unified multi-granularity comprehension and generation. *arXiv preprint arXiv:2404.14396*, 2024.

Jianping Gou, Baosheng Yu, Stephen J Maybank, and Dacheng Tao. Knowledge distillation: A survey. *International journal of computer vision*, 129(6):1789–1819, 2021.

Yash Goyal, Tejas Khot, Douglas Summers-Stay, Dhruv Batra, and Devi Parikh. Making the v in vqa matter: Elevating the role of image understanding in visual question answering. In *Proceedings of the IEEE conference on computer vision and pattern recognition*, pp. 6904–6913, 2017.

Daya Guo, Dejian Yang, Haowei Zhang, Junxiao Song, Ruoyu Zhang, Runxin Xu, Qihao Zhu, Shirong Ma, Peiyi Wang, Xiao Bi, et al. Deepseek-r1: Incentivizing reasoning capability in llms via reinforcement learning. *arXiv preprint arXiv:2501.12948*, 2025.

Danna Gurari, Qing Li, Abigale J Stangl, Anhong Guo, Chi Lin, Kristen Grauman, Jiebo Luo, and Jeffrey P Bigham. Vizwiz grand challenge: Answering visual questions from blind people. In *Proceedings of the IEEE conference on computer vision and pattern recognition*, pp. 3608–3617, 2018.

Jinghan He, Haiyun Guo, Ming Tang, and Jinqiao Wang. Continual instruction tuning for large multimodal models. *arXiv preprint arXiv:2311.16206*, 2023.

Xuehai He, Yichen Zhang, Luntian Mou, Eric Xing, and Pengtao Xie. Pathvqa: 30000+ questions for medical visual question answering. *arXiv preprint arXiv:2003.10286*, 2020.

Geoffrey Hinton, Oriol Vinyals, and Jeff Dean. Distilling the knowledge in a neural network. *arXiv preprint arXiv:1503.02531*, 2015.

Edward J Hu, Yelong Shen, Phillip Wallis, Zeyuan Allen-Zhu, Yuanzhi Li, Shean Wang, Lu Wang, Weizhu Chen, et al. Lora: Low-rank adaptation of large language models. *ICLR*, 1(2):3, 2022.

Zehao Huang and Naiyan Wang. Like what you like: Knowledge distill via neuron selectivity transfer. *arXiv preprint arXiv:1707.01219*, 2017.

Drew A Hudson and Christopher D Manning. Gqa: A new dataset for real-world visual reasoning and compositional question answering. In *Proceedings of the IEEE/CVF conference on computer vision and pattern recognition*, pp. 6700–6709, 2019.

Saurav Jha, Dong Gong, and Lina Yao. Clap4clip: Continual learning with probabilistic finetuning for vision-language models. *Advances in neural information processing systems*, 37:129146–129186, 2024.

James Kirkpatrick, Razvan Pascanu, Neil Rabinowitz, Joel Veness, Guillaume Desjardins, Andrei A Rusu, Kieran Milan, John Quan, Tiago Ramalho, Agnieszka Grabska-Barwinska, et al. Overcoming catastrophic forgetting in neural networks. *Proceedings of the national academy of sciences*, 114(13):3521–3526, 2017.

Alex Krizhevsky, Geoffrey Hinton, et al. Learning multiple layers of features from tiny images, 2009.

Kartik Kuckreja, Muhammad Sohail Danish, Muzammal Naseer, Abhijit Das, Salman Khan, and Fahad Shahbaz Khan. Geochat: Grounded large vision-language model for remote sensing. In *Proceedings of the IEEE/CVF Conference on Computer Vision and Pattern Recognition*, pp. 27831–27840, 2024.

Feng Li, Renrui Zhang, Hao Zhang, Yuanhan Zhang, Bo Li, Wei Li, Zejun Ma, and Chunyuan Li. Llava-next-interleave: Tackling multi-image, video, and 3d in large multimodal models. *arXiv preprint arXiv:2407.07895*, 2024a.

Lei Li, Yuqi Wang, Runxin Xu, Peiyi Wang, Xiachong Feng, Lingpeng Kong, and Qi Liu. Multimodal arxiv: A dataset for improving scientific comprehension of large vision-language models. *arXiv preprint arXiv:2403.00231*, 2024b.

Zhizhong Li and Derek Hoiem. Learning without forgetting. *IEEE transactions on pattern analysis and machine intelligence*, 40(12):2935–2947, 2017.

Adam Dahlgren Lindström and Savitha Sam Abraham. Clevr-math: A dataset for compositional language, visual and mathematical reasoning. *arXiv preprint arXiv:2208.05358*, 2022.

Chenxiao Liu and Xiaojun Wan. Codeqa: A question answering dataset for source code comprehension. *arXiv preprint arXiv:2109.08365*, 2021.

Haotian Liu, Chunyuan Li, Qingyang Wu, and Yong Jae Lee. Visual instruction tuning. *Advances in neural information processing systems*, 36:34892–34916, 2023.

Haotian Liu, Chunyuan Li, Yuheng Li, and Yong Jae Lee. Improved baselines with visual instruction tuning. In *Proceedings of the IEEE/CVF conference on computer vision and pattern recognition*, pp. 26296–26306, 2024.

David Lopez-Paz and Marc'Aurelio Ranzato. Gradient episodic memory for continual learning. *Advances in neural information processing systems*, 30, 2017.

Haoyu Lu, Wen Liu, Bo Zhang, Bingxuan Wang, Kai Dong, Bo Liu, Jingxiang Sun, Tongzheng Ren, Zhuoshu Li, Hao Yang, et al. Deepseek-vl: towards real-world vision-language understanding. *arXiv preprint arXiv:2403.05525*, 2024.

Pan Lu, Liang Qiu, Jiaqi Chen, Tony Xia, Yizhou Zhao, Wei Zhang, Zhou Yu, Xiaodan Liang, and Song-Chun Zhu. Iconqa: A new benchmark for abstract diagram understanding and visual language reasoning. *arXiv preprint arXiv:2110.13214*, 2021.

Pan Lu, Swaroop Mishra, Tanglin Xia, Liang Qiu, Kai-Wei Chang, Song-Chun Zhu, Oyvind Tafjord, Peter Clark, and Ashwin Kalyan. Learn to explain: Multimodal reasoning via thought chains for science question answering. *Advances in Neural Information Processing Systems*, 35:2507–2521, 2022.

Yun Luo, Zhen Yang, Fandong Meng, Yafu Li, Jie Zhou, and Yue Zhang. An empirical study of catastrophic forgetting in large language models during continual fine-tuning. *arXiv preprint arXiv:2308.08747*, 2023.

Junhua Mao, Jonathan Huang, Alexander Toshev, Oana Camburu, Alan L Yuille, and Kevin Murphy. Generation and comprehension of unambiguous object descriptions. In *Proceedings of the IEEE conference on computer vision and pattern recognition*, pp. 11–20, 2016.

Ahmed Masry, Do Xuan Long, Jia Qing Tan, Shafiq Joty, and Enamul Hoque. Chartqa: A benchmark for question answering about charts with visual and logical reasoning. *arXiv preprint arXiv:2203.10244*, 2022.

Minesh Mathew, Dimosthenis Karatzas, and CV Jawahar. Docvqa: A dataset for vqa on document images. In *Proceedings of the IEEE/CVF winter conference on applications of computer vision*, pp. 2200–2209, 2021.

Anand Mishra, Shashank Shekhar, Ajeet Kumar Singh, and Anirban Chakraborty. Ocr-vqa: Visual question answering by reading text in images. In *2019 international conference on document analysis and recognition (ICDAR)*, pp. 947–952. IEEE, 2019.

Xingchao Peng, Qinxun Bai, Xide Xia, Zijun Huang, Kate Saenko, and Bo Wang. Moment matching for multi-source domain adaptation. In *Proceedings of the IEEE/CVF international conference on computer vision*, pp. 1406–1415, 2019.

Bryan A Plummer, Liwei Wang, Chris M Cervantes, Juan C Caicedo, Julia Hockenmaier, and Svetlana Lazebnik. Flickr30k entities: Collecting region-to-phrase correspondences for richer image-to-sentence models. In *Proceedings of the IEEE international conference on computer vision*, pp. 2641–2649, 2015.

Jingyang Qiao, Xin Tan, Yanyun Qu, Shouhong Ding, Yuan Xie, et al. Large continual instruction assistant. In *Forty-second International Conference on Machine Learning*, 2025a.

Jingyang Qiao, Zhizhong Zhang, Xin Tan, Yanyun Qu, Wensheng Zhang, Zhi Han, and Yuan Xie. Gradient projection for continual parameter-efficient tuning. *IEEE Transactions on Pattern Analysis and Machine Intelligence*, 2025b.

Alec Radford, Jong Wook Kim, Chris Hallacy, Aditya Ramesh, Gabriel Goh, Sandhini Agarwal, Girish Sastry, Amanda Askell, Pamela Mishkin, Jack Clark, et al. Learning transferable visual models from natural language supervision. In *International conference on machine learning*, pp. 8748–8763. PmLR, 2021.

Nils Reimers and Iryna Gurevych. Sentence-bert: Sentence embeddings using siamese bert-networks. *arXiv preprint arXiv:1908.10084*, 2019.

David Rolnick, Arun Ahuja, Jonathan Schwarz, Timothy Lillicrap, and Gregory Wayne. Experience replay for continual learning. *Advances in neural information processing systems*, 32, 2019.

Olga Russakovsky, Jia Deng, Hao Su, Jonathan Krause, Sanjeev Satheesh, Sean Ma, Zhiheng Huang, Andrej Karpathy, Aditya Khosla, Michael Bernstein, et al. Imagenet large scale visual recognition challenge. *International journal of computer vision*, 115(3):211–252, 2015.

Thomas Scialom, Tuhin Chakrabarty, and Smaranda Muresan. Fine-tuned language models are continual learners. *arXiv preprint arXiv:2205.12393*, 2022.

Amanpreet Singh, Vivek Natarajan, Meet Shah, Yu Jiang, Xinlei Chen, Dhruv Batra, Devi Parikh, and Marcus Rohrbach. Towards vqa models that can read. In *Proceedings of the IEEE/CVF conference on computer vision and pattern recognition*, pp. 8317–8326, 2019.

James Seale Smith, Yen-Chang Hsu, Lingyu Zhang, Ting Hua, Zsolt Kira, Yilin Shen, and Hongxia Jin. Continual diffusion: Continual customization of text-to-image diffusion with c-lora. *arXiv preprint arXiv:2304.06027*, 2023a.

James Seale Smith, Leonid Karlinsky, Vyshnavi Gutta, Paola Cascante-Bonilla, Donghyun Kim, Assaf Arbelle, Rameswar Panda, Rogerio Feris, and Zsolt Kira. Coda-prompt: Continual decomposed attention-based prompting for rehearsal-free continual learning. In *Proceedings of the IEEE/CVF conference on computer vision and pattern recognition*, pp. 11909–11919, 2023b.

Sakthivel Srinivasan, Iyo Koyanagi, Pablo Vergara, Yuteng Wang, Akinobu Ohba, Toshie Naoi, Kaspar E Vogt, Yoan Chérasse, Noriki Kutsumura, Takeshi Sakurai, et al. Transient reactivation of small ensembles of adult-born neurons during rem sleep supports memory consolidation in mice. *Nature Communications*, 16(1):7210, 2025.

Robert Stickgold. Sleep-dependent memory consolidation. *Nature*, 437(7063):1272–1278, 2005.

Chameleon Team. Chameleon: Mixed-modal early-fusion foundation models. *arXiv preprint arXiv:2405.09818*, 2024.

Hugo Touvron, Thibaut Lavril, Gautier Izacard, Xavier Martinet, Marie-Anne Lachaux, Timothée Lacroix, Baptiste Rozière, Naman Goyal, Eric Hambro, Faisal Azhar, et al. Llama: Open and efficient foundation language models. *arXiv preprint arXiv:2302.13971*, 2023a.

Hugo Touvron, Louis Martin, Kevin Stone, Peter Albert, Amjad Almahairi, Yasmine Babaei, Nikolay Bashlykov, Soumya Batra, Prajjwal Bhargava, Shruti Bhosale, et al. Llama 2: Open foundation and fine-tuned chat models. *arXiv preprint arXiv:2307.09288*, 2023b.

Xinlong Wang, Xiaosong Zhang, Zhengxiong Luo, Quan Sun, Yufeng Cui, Jinsheng Wang, Fan Zhang, Yueze Wang, Zhen Li, Qiying Yu, et al. Emu3: Next-token prediction is all you need. *arXiv preprint arXiv:2409.18869*, 2024.

Yabin Wang, Zhiwu Huang, and Xiaopeng Hong. S-prompts learning with pre-trained transformers: An occam's razor for domain incremental learning. *Advances in Neural Information Processing Systems*, 35:5682–5695, 2022a.

Zifeng Wang, Zizhao Zhang, Sayna Ebrahimi, Ruoxi Sun, Han Zhang, Chen-Yu Lee, Xiaoqi Ren, Guolong Su, Vincent Perot, Jennifer Dy, et al. Dualprompt: Complementary prompting for rehearsal-free continual learning. In *European conference on computer vision*, pp. 631–648. Springer, 2022b.

Zifeng Wang, Zizhao Zhang, Chen-Yu Lee, Han Zhang, Ruoxi Sun, Xiaoqi Ren, Guolong Su, Vincent Perot, Jennifer Dy, and Tomas Pfister. Learning to prompt for continual learning. In *Proceedings of the IEEE/CVF conference on computer vision and pattern recognition*, pp. 139–149, 2022c.

Matthew A Wilson and Bruce L McNaughton. Reactivation of hippocampal ensemble memories during sleep. *Science*, 265(5172):676–679, 1994.

Yuan Xie, Jingyang Qiao, Weicheng Meng, Qingsong Hu, Jie Jin, Zhizhong Zhang, Xin Tan, and Jingyu Gong. Continual-next: A toolbox of multimodal continual instruction tuning, August 2025. URL https://github.com/ECNU-SII/Continual-NExT.

Shipeng Yan, Jiangwei Xie, and Xuming He. Der: Dynamically expandable representation for class incremental learning. In *Proceedings of the IEEE/CVF conference on computer vision and pattern recognition*, pp. 3014–3023, 2021.

An Yang, Baosong Yang, Beichen Zhang, Binyuan Hui, Bo Zheng, Bowen Yu, Chengyuan Li, Dayiheng Liu, Fei Huang, Haoran Wei, Huan Lin, Jian Yang, Jianhong Tu, Jianwei Zhang, Jianxin Yang, Jiaxi Yang, Jingren Zhou, Junyang Lin, Kai Dang, Keming Lu, Keqin Bao, Kexin Yang, Le Yu, Mei Li, Mingfeng Xue, Pei Zhang, Qin Zhu, Rui Men, Runji Lin, Tianhao Li, Tianyi Tang, Tingyu Xia, Xingzhang Ren, Xuancheng Ren, Yang Fan, Yang Su, Yichang Zhang, Yu Wan, Yuqiong Liu, Zeyu Cui, Zhenru Zhang, and Zihan Qiu. Qwen2.5 technical report, 2025. URL https://arxiv.org/abs/2412.15115.

Yi Yang, Wen-tau Yih, and Christopher Meek. Wikiqa: A challenge dataset for open-domain question answering. In *Proceedings of the 2015 conference on empirical methods in natural language processing*, pp. 2013–2018, 2015.

Jaehong Yoon, Divyam Madaan, Eunho Yang, and Sung Ju Hwang. Online coreset selection for rehearsal-based continual learning. *arXiv preprint arXiv:2106.01085*, 2021.

Dianzhi Yu, Xinni Zhang, Yankai Chen, Aiwei Liu, Yifei Zhang, Philip S Yu, and Irwin King. Recent advances of multimodal continual learning: A comprehensive survey. *arXiv preprint arXiv:2410.05352*, 2024a.

Jiazuo Yu, Yunzhi Zhuge, Lu Zhang, Ping Hu, Dong Wang, Huchuan Lu, and You He. Boosting continual learning of vision-language models via mixture-of-experts adapters. In *Proceedings of the IEEE/CVF Conference on Computer Vision and Pattern Recognition*, pp. 23219–23230, 2024b.

Yahan Yu, Duzhen Zhang, Yong Ren, Xuanle Zhao, Xiuyi Chen, and Chenhui Chu. Progressive LoRA for multimodal continual instruction tuning. In Wanxiang Che, Joyce Nabende, Ekaterina Shutova, and Mohammad Taher Pilehvar (eds.), *Findings of the Association for Computational Linguistics: ACL 2025*, pp. 2779–2796, Vienna, Austria, July 2025. Association for Computational Linguistics. ISBN 979-8-89176-256-5. doi: 10.18653/v1/2025.findings-acl.143. URL https://aclanthology.org/2025.findings-acl.143/.

Jun Zhan, Junqi Dai, Jiasheng Ye, Yunhua Zhou, Dong Zhang, Zhigeng Liu, Xin Zhang, Ruibin Yuan, Ge Zhang, Linyang Li, et al. Anygpt: Unified multimodal llm with discrete sequence modeling. *arXiv preprint arXiv:2402.12226*, 2024.

Qingru Zhang, Minshuo Chen, Alexander Bukharin, Nikos Karampatziakis, Pengcheng He, Yu Cheng, Weizhu Chen, and Tuo Zhao. Adalora: Adaptive budget allocation for parameter-efficient fine-tuning. *arXiv preprint arXiv:2303.10512*, 2023.

Xinni Zhang, Yankai Chen, Chenhao Ma, Yixiang Fang, and Irwin King. Influential exemplar replay for incremental learning in recommender systems. In *Proceedings of the AAAI Conference on Artificial Intelligence*, volume 38, pp. 9368–9376, 2024.

Kaizhi Zheng, Xuehai He, and Xin Eric Wang. Minigpt-5: Interleaved vision-and-language generation via generative vokens. *arXiv preprint arXiv:2310.02239*, 2023.

Deyao Zhu, Jun Chen, Xiaoqian Shen, Xiang Li, and Mohamed Elhoseiny. Minigpt-4: Enhancing vision-language understanding with advanced large language models. *arXiv preprint arXiv:2304.10592*, 2023.

Didi Zhu, Zhongyi Sun, Zexi Li, Tao Shen, Ke Yan, Shouhong Ding, Kun Kuang, and Chao Wu. Model tailor: Mitigating catastrophic forgetting in multi-modal large language models. *arXiv preprint arXiv:2402.12048*, 2024.

A SUPPLEMENTARY RESULTS OF CONTINUAL INSTRUCTION TUNING

Table 8: Comparisons with baselines on LLaVA-1.5-13B, CoIN benchmark.

Method	Venue	Accuracy on Each Task								Overall Results		
		1-ScienceQA	2-TextVQA	3-ImageNet	4-GQA	5-VizWiz	6-Grounding	7-VQAv2	8-OCRVQA	Avg.ACC(↑)	Forgetting(↓)	New.ACC(↑)
LoRA (Hu et al., 2022)	ICLR'22	60.03	41.19	10.62	31.03	32.67	2.60	46.33	61.00	35.68	32.90	64.47
MT (Zhu et al., 2024)	ICML'24	80.43	60.72	46.70	60.35	49.19	33.16	63.74	65.44	57.47	11.26	67.32
PGP (Qiao et al., 2025b)	ICLR'24	82.50	60.64	49.15	62.53	49.43	37.37	65.57	65.82	59.13	10.11	67.98
EProj (He et al., 2023)	ArXiv'23	77.65	58.93	92.31	60.22	38.27	33.77	64.39	65.80	61.42	5.84	66.53
CIA (Qiao et al., 2025a)	ICLR'24	83.94	61.40	97.05	62.61	43.99	39.72	66.29	65.78	65.10	2.31	67.12
Ours	-	**83.82**	**61.99**	**93.98**	**59.49**	**57.98**	**36.03**	**66.09**	**64.67**	**65.51**	**2.08**	**67.32**

Table 9: Comparisons with baselines on Qwen-VL, CoIN benchmark.

Method	Venue	Accuracy on Each Task								Overall Results		
		1-ScienceQA	2-TextVQA	3-ImageNet	4-GQA	5-VizWiz	6-Grounding	7-VQAv2	8-OCRVQA	Avg.ACC(↑)	Forgetting(↓)	New.ACC(↑)
LoRA (Hu et al., 2022)	ICLR'22	31.05	42.45	29.57	55.57	15.30	40.33	67.75	47.80	41.23	19.36	58.17
EWC (Kirkpatrick et al., 2017)	PNAS'17	64.30	58.67	44.04	57.73	38.16	48.04	66.98	41.76	52.46	8.68	60.06
PGP (Qiao et al., 2025b)	ICLR'24	66.42	41.33	32.16	49.83	36.05	24.22	58.60	43.96	44.07	5.90	48.30
Ours	-	**77.84**	**65.36**	**67.84**	**60.47**	**53.83**	**68.54**	**69.37**	**61.42**	**65.58**	**4.21**	**69.27**

Table 10: Comparisons with baselines on Qwen2.5-VL-Instruct, Continual-NExT benchmark.

Method	Venue	Accuracy on Each Task & Overall Results								
		1-ArxivQA	2-GeoChat	3-IconQA	4-ClevrMath	5-CodeQA	6-ImageNet	7-Flickr30k	8-DocVQA	9-TextVQA
Zero-shot	-	70.23	67.53	28.60	81.93	3.63	35.62	8.97	82.09	68.94
LoRA (Hu et al., 2022)	ICLR'22	71.39	89.00	73.40	96.80	2.05	78.77	20.92	85.04	68.94
LwF (Li & Hoiem, 2017)	TPAMI'16	72.60	92.33	58.56	95.40	3.49	76.53	21.42	83.77	71.86
EWC (Kirkpatrick et al., 2017)	PNAS'17	73.28	92.00	67.87	89.20	3.53	76.06	20.53	80.61	53.82
Replay (Rolnick et al., 2019)	NIPS'19	71.37	87.57	78.37	98.83	2.45	83.29	20.81	86.32	71.28
MoELoRA (Chen et al., 2024a)	NIPS'24	72.19	91.53	74.36	97.66	2.65	90.75	21.08	85.51	79.55
PCLR	-	**74.72**	**92.13**	**88.10**	**97.27**	**8.45**	**74.06**	**21.93**	**86.27**	**80.63**
PCLR-LwF (PCLR variant)	-	**74.43**	**92.23**	**88.60**	**97.80**	**8.93**	**88.42**	**20.75**	**86.19**	**80.38**
		10-MathQA	11-ChartQA	12-PathVQA	13-Grounding	14-ScienceQA	15-WikiQA	Avg.ACC(↑)	Forgetting(↓)	New.ACC(↑)
Zero-shot	-	0.03	75.00	33.22	72.23	82.95	2.90	47.59	-	-
LoRA (Hu et al., 2022)	ICLR'22	34.81	73.88	7.96	86.60	80.08	4.87	58.30	9.36	67.04
LwF (Li & Hoiem, 2017)	TPAMI'16	50.72	67.28	7.57	87.60	91.44	16.27	59.79	10.98	70.04
EWC (Kirkpatrick et al., 2017)	PNAS'17	48.31	67.36	13.26	86.99	87.05	15.64	58.37	11.89	69.47
Replay (Rolnick et al., 2019)	NIPS'19	45.50	74.72	8.66	86.11	90.90	16.11	61.49	6.40	67.46
MoELoRA (Chen et al., 2024a)	NIPS'24	2.14	74.80	6.35	87.68	80.90	16.90	58.94	11.81	69.96
PCLR	-	**42.85**	**76.76**	**39.44**	**86.24**	**87.27**	**7.74**	**64.26**	**5.18**	**69.08**
PCLR-LwF (PCLR variant)	-	**45.16**	**76.08**	**44.43**	**85.53**	**88.38**	**9.32**	**65.78**	**3.74**	**69.26**

As shown in Table 8, we discover that PCLR achieves the highest overall performance on the CoIN benchmark, LLaVA-1.5-13B. Compared to the former best regularization method PGP (Qiao et al., 2025b), the Avg.ACC improves by 6.38 and the Forgetting decreases by 8.03, demonstrating strong continual learning ability. Furthermore, our method outperforms the extension methods Eproj (He et al., 2023) and CIA (Qiao et al., 2025a). Experimental results show that our method is robust across model scales and maintains strong performance on larger and powerful models.

As shown in Table 9, we discover that PCLR achieves the highest overall performance on the CoIN benchmark, Qwen-VL. Compared to the former best regularization method EWC (Kirkpatrick et al., 2017), the Avg.ACC improves by 13.12 and the Forgetting decreases by 4.47, demonstrating strong continual learning ability. Experimental results show that our method is robust across models of different architectures and maintains strong performance even when the base architecture varies.

As shown in Table 10, our method exceeds the best of other methods (Replay), improving Avg.ACC by 2.77 and reducing Forgetting by 1.22, which demonstrates that PCLR sustains strong performance on the long-term Continual-NExT benchmark, Qwen2.5-VL-Instruct. Similar to the main paper, we introduce PCLR-LwF, which divides the whole task sequence into five consecutive groups, and applies LwF in each group. This integration with simple baseline yields notable gains by improving Avg.ACC by 1.52 and reducing Forgetting by 1.44, while preserving the same parameter number as PCLR.

In summary, extensive experiments on Large Multimodal Models (LMMs), including LLaVA-1.5-7B, LLaVA-1.5-13B and Qwen-VL on the CoIN benchmark, LLaVA-1.5-hf and Qwen2.5-VL-Instruct on the Continual-NExT benchmark, demonstrate the superiority of PCLR. The method achieves an effective balance between plasticity, stability and memory efficiency. Importantly, PCLR prevents unbounded parameter growth via the Compression–Integration–Learning (CIL) pipeline. Moreover, its modular design enables seamless integration with regularization methods such as LwF, as demonstrated by the PCLR-LwF variant, which further improves training efficiency without sacrificing performance. These results establish PCLR as a scalable, efficient and robust framework for multimodal continual instruction tuning in LMMs.

B Details of Experimental Setting

Overall Setting: For each dataset, we set the training epoch to 1. The LLM backbone and cross-modal modules are incorporated into the PCLR framework. Throughout all phases, only the inserted PCLR modules are trainable, and the LMM remains frozen. During learning, the learning rate is set to 2×10^{-4} for LLaVA series, 2×10^{-5} for Qwen-VL, 1×10^{-4} for Qwen2.5-VL-Instruct. During integration, only data from the current task is used, the learning rate is set to 5×10^{-5} for LLaVA-1.5, 1×10^{-5} for Qwen-VL, while 2×10^{-6} for LLaVA-1.5-hf and Qwen2.5-VL-Instruct. Weight decay is set to 0. The maximum input embedding length is fixed as 2048. We employ gradient checkpointing and mixed-precision training using TF32 and BF16. We use DeepSpeed ZeRO-2 for distributed training. All experiments are conducted on 4×80-GB GPUs. During learning, we employ a rank-64 extension and later switch to a rank-32 extension. During compression, we adopt a retention rate of 100% (no compression) for the first three tasks, then set it to 75%, and finally adjust it to 87.5%.

LoRA Rank Configuration: In the main paper, all baselines are fine-tuned using LoRA with rank 128. However, due to the MoE architecture of PCLR, it is infeasible to ensure a fair comparison of both total and activated ranks simultaneously. To balance parameter efficiency and memory cost while preserving the MoE structure, we adopt: total rank 256, activated rank 64 (activated during forward passes in both training and inference), and optional shared rank 32 (activated during forward passes in both training and inference, trainable during Integration and frozen during Learning). This setting balances total rank and activated rank to maximize overall fairness.

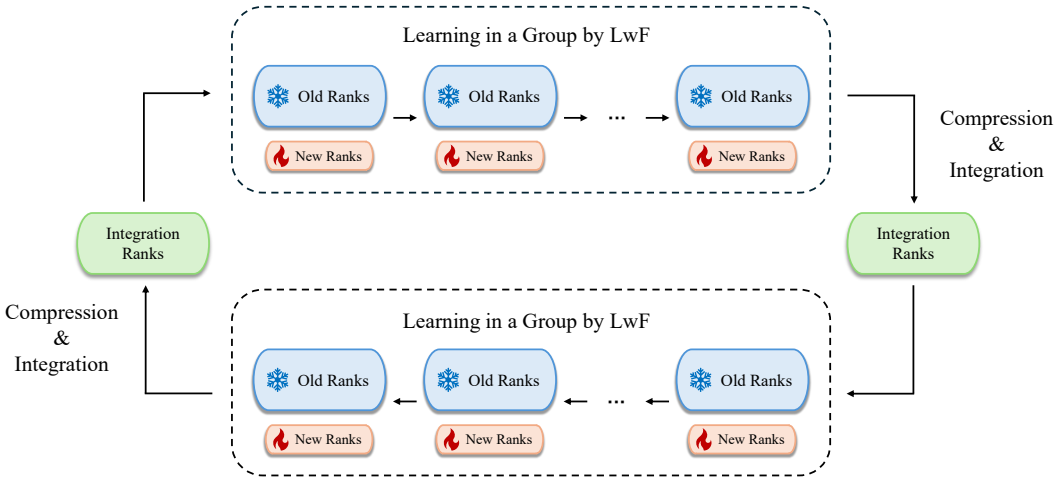

Figure 5: PCLR-LwF Overview. In long-term CIT, the task sequence is divided into several groups, with the tasks in each group being contiguous in the original sequence. Within each group, we apply LwF for learning. Between the groups, the CIL process is adopted.

Combination with LwF: In the main paper, we propose an optimization for long-term continual instruction tuning: instead of running CIL after each task, we perform constrained updates in the newly extended rank space using regularization methods such as LwF (Li & Hoiem, 2017), for a subset of tasks. As described in the main paper, on the Continual-NExT benchmark, we group consecutive tasks into a cluster and apply LwF for constrained updates within each cluster, with a weight of 0.1. This approach reduces training cost and improves performance while maintaining the same total rank as the standard PCLR. The PCLR-LwF pipeline is shown in figure 5.

Equivalent Setting for Fake Query Sampling: The main paper states that fake queries are sampled from the key pool. However, during continual compression, the number of keys from earlier tasks decays exponentially. This produces unfair sampling of synthetic task-related queries. After completing each task, we average its newly generated keys and place the resulting mean vector into a global task key pool. Each task thus retains a single representative fake query, which keeps cross-task sampling balanced during the integration.

C THE CASES OF CONTINUAL INSTRUCTION TUNING

In this section, we present evaluation cases after completing the CoIN (Chen et al., 2024a) benchmark by using Pretrain, MoELoRA, PCLR, and Ground-Truth.

Model after continual tuning, test on ScienceQA

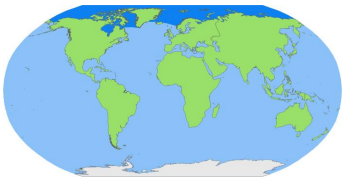

Q: Which ocean is highlighted?
A.the Atlantic Ocean
B.the Indian Ocean
C.the Arctic Ocean
D.the Southern Ocean
Answer with the option's letter from the given choices directly.

A: Answer from Pretrain
The correct answer is C. the Arctic Ocean.

A: Answer from MoELoRA
A

A: Answer from PCLR
C

A: Answer from Ground-Truth
C

Model after continual tuning, test on TextVQA

Q: Which centre is featured on the plane?
Reference OCR token: FXQ, THE, SOARING, CENTRE, HUSBANDS, BOSWORTH, PuCHACZ
Answer the question using a single word or phrase.

A: Answer from Pretrain
The plane features the FXQ centre.

A: Answer from MoELoRA
Soaring Centre Husband & Bosworth

A: Answer from PCLR
soaring centre

A: Answer from Ground-Truth
the soaring centre

Model after continual tuning, test on ImageNet

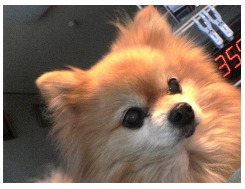

Q: What is the object in the image?
Give the object in the image in the form of a single word or a concise phrase.

A: Answer from Pretrain
The object in the image is a dog.

A: Answer from MoELoRA
dog.

A: Answer from PCLR
Pomeranian.

A: Answer from Ground-Truth
Pomeranian

Figure 6: From top to bottom, these are cases on ScienceQA, TextVQA, and ImageNet after learning the final task of the CoIN benchmark.

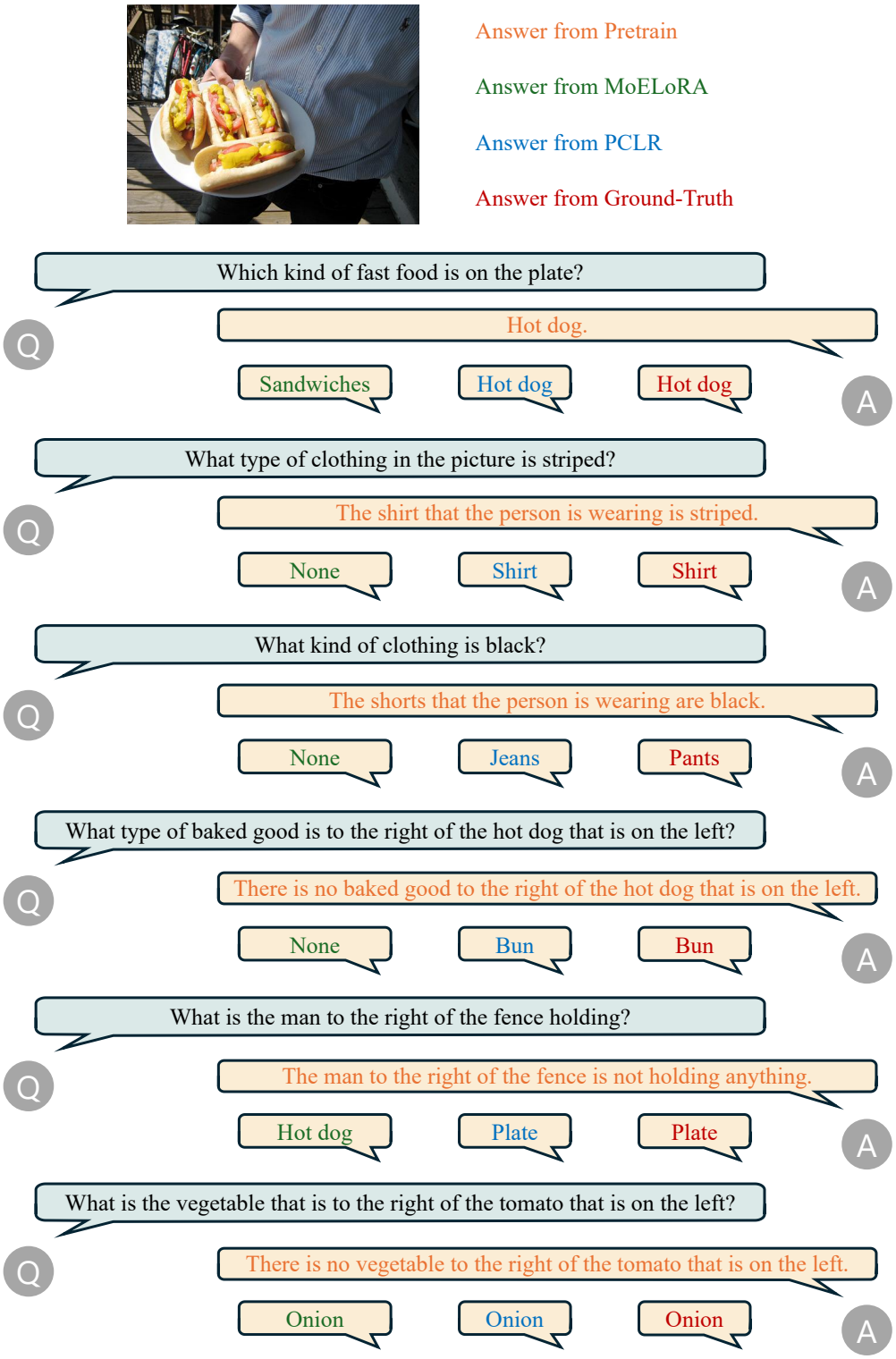

Figure 7: The case on GQA after learning the final task of the CoIN benchmark. This is a case of multiple rounds of dialogue.

Model after continual tuning, test on VizWiz

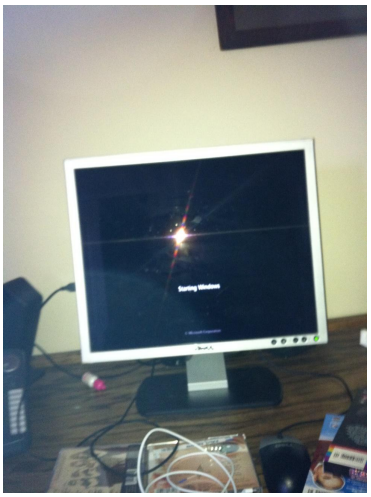

Question1: Can you tell me what the error message is on the Windows screen?
When the provided information is insufficient, respond with 'unanswerable'.
Answer the question using a single word or phrase.

Pretrain: unanswerable
MoELoRA: unanswerable
PCLR: **starting windows**
Ground-Truth: starting windows

Question2: What is the title of this book?

Pretrain: I'm sorry, but I cannot answer your question as there is no book visible in the provided image. Please provide a different image or question.
MoELoRA: Windows 7: The Missing Manual
PCLR: **unanswerable**
Ground-Truth: unanswerable

Model after continual tuning, test on Grounding

Question1: Identify and provide the coordinates of the bounding box described in the sentence: bananas in the middle.

Pretrain: I'm sorry, but I cannot provide the bounding box coordinates for the sentence \"bananas in the middle\" as it is not clear what region or object is being described. Please provide more context or a specific sentence for me to assist you.
MoELoRA: [0.4,0.52,0.61,0.69]
PCLR: **[0.32,0.39,0.67,0.76]**
Ground-Truth: [0.35,0.4,0.64,0.76]

Question2: Give the bounding box coordinates as described in the sentence: top left bunch.

Pretrain: I'm sorry, but I cannot provide the bounding box coordinates for the sentence \"top left bunch\" as it is not clear what region or object is being described. Please provide more context or a specific sentence for me to assist you.
MoELoRA: [0.4,0.52,0.61,0.69]
PCLR: **[0.0,0.24,0.25,0.49]**
Ground-Truth: [0.0,0.22,0.24,0.4]

Figure 8: From top to bottom, these are cases on VizWiz and Grounding after learning the final task of the CoIN benchmark.

D LAYER SENSITIVITY ANALYSIS IN PCLR

In this section, we investigate the sensitivity of different LMM layers to compression and integration in PCLR for continual learning. Based on the 40-layer LLaVA-1.5-13B Transformer architecture, we divide it into 5 groups of 8 consecutive layers (Lower: layers 1–8, Middle-Lower: layers 9–16, Middle: layers 17–24, Middle-Upper: layers 25–32, Upper: layers 33–40). In each experiment, we skip the Compression and Integration stages for one group (opened group), while keeping the other four groups unchanged. The results in Table 11 show that task-specific sensitivity varies across layers, with the highest performance degradation observed in upper layers compression (-0.53@Avg.ACC) and the lowest in mid-level layers compression (-0.15@Avg.ACC). This observation highlights the layer-specific characteristics in PCLR.

Table 11: The results of LLaVA-1.5-13B on **different opened groups**.

Layers	**Accuracy on Each Task**								**Evaluation Metrics**	
	ScienceQA	TextVQA	ImageNet	GQA	VizWiz	Grounding	VQAV2	OCRVQA	Avg.ACC	Forgetting
Origin	83.82	61.99	93.98	59.49	57.98	36.03	66.09	64.67	65.51	2.08
Lower	86.02	62.28	94.28	60.40	56.80	35.33	66.51	63.99	65.70	1.56
Middle-Lower	86.02	63.18	94.59	60.43	56.54	36.21	66.05	62.93	65.74	1.36
Middle	83.99	62.49	94.89	59.87	58.76	34.93	66.14	64.19	65.66	1.73
Middle-Upper	83.80	62.04	95.07	59.58	58.44	36.70	66.16	64.31	65.76	1.67
Upper	83.85	61.89	96.46	60.02	59.23	36.13	66.15	64.56	66.04	1.32

We hypothesize that lower layers focus on input comprehension, mid-level layers focus on reasoning, and upper layers focus on instruction-following output generation. Since reasoning processes across tasks often share a high degree of similarity (general logic patterns), mid-level compression causes minimal interference. However, upper layers face significant task-specific divergence in output generation (single-choice answers in ScienceQA *v.s.* classification answers in ImageNet *v.s.* bounding-box answers in Grounding), leading to pronounced conflicts during compression-integration. Notably, the compression of lower layers is especially sensitive to ScienceQA because its inputs mix text-only and image–text samples, unlike tasks that are exclusively image–text. This indicates that heterogeneous modality distributions can amplify compression-induced performance drops in the lower layers.

Our findings motivate a **layer-aware compression strategy** for future CIL optimization: applying maximal compression retention ratio to upper layers (high conflict), moderate compression retention ratio to lower layers (moderate conflict), and minimal compression retention ratio to mid-level layers (low conflict). This optimization is expected to achieve further performance improvements while maintaining a similar memory budget.

E EVALUATION METRICS

We emphasize that our evaluation of prediction accuracy is based on a comparison between the outputs of LMMs and the corresponding ground-truth annotations. This evaluation protocol in Chen et al. (2024a), provides a rigorous and consistent criterion. For short textual outputs we apply **Truth Alignment**, and for longer textual outputs we compute semantic similarity using Sentence-Transformers (Reimers & Gurevych, 2019) and accept when the similarity score is at least 0.8.

We adopt 3 primary metrics to comprehensively evaluate continual instruction tuning performance:

Average Accuracy (Avg.ACC) measures the average test accuracy across all datasets, reflecting the overall performance of models throughout the continual learning process.

Forgetting (FOR) quantifies the decline in performance on previously learned datasets after training on new datasets. It serves as an indicator of **stability** (retaining previous knowledge).

New Accuracy (New.ACC) computes the average test accuracy on newly introduced datasets. It serves as an indicator of **plasticity** (adapting to new tasks).

Overall, these metrics are generally defined as follows:

$$\text{Avg.ACC} = \frac{1}{T}\sum_{i=1}^{T} A_{T,i}, \tag{8}$$

$$\text{FOR} = \frac{1}{T-1}\sum_{i=1}^{T-1}\left(\max_{j\in[i,T]} A_{j,i} - A_{T,i}\right), \tag{9}$$

$$\text{New.ACC} = \frac{1}{T}\sum_{i=1}^{T} A_{i,i}, \tag{10}$$

where T denotes the total number of datasets, $A_{T,i}$ represents the accuracy of the i-th dataset evaluated on the model after training on the T-th (final) dataset, $A_{j,i}$ is the accuracy of the i-th dataset on the model after training on the j-th dataset, and $A_{i,i}$ is the accuracy of the i-th dataset evaluated immediately after its own training.

F Visualization of Expert Transition during CIT

In this section, we visualize the expert transition process during continual instruction tuning (CIT) within the PCLR method. We follow the task sequence defined by the CoIN benchmark: ScienceQA → TextVQA → ImageNet → GQA → VizWiz → Grounding → VQAv2 → OCRVQA. We present the rank experts activation patterns on the last five tasks. Specifically, the invocation rate of the rank experts on the current task and previously learned tasks is shown as below.

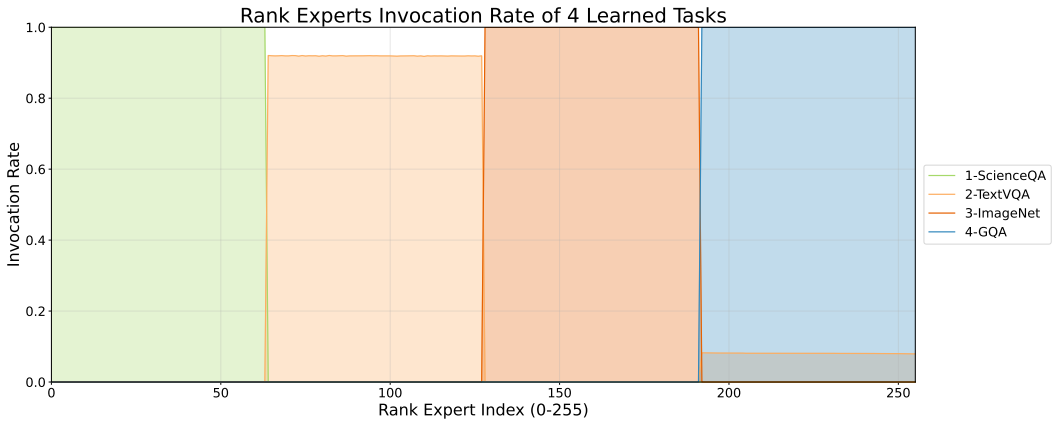

Figure 9: The invocation rate of rank experts after learning the 4-th task GQA.

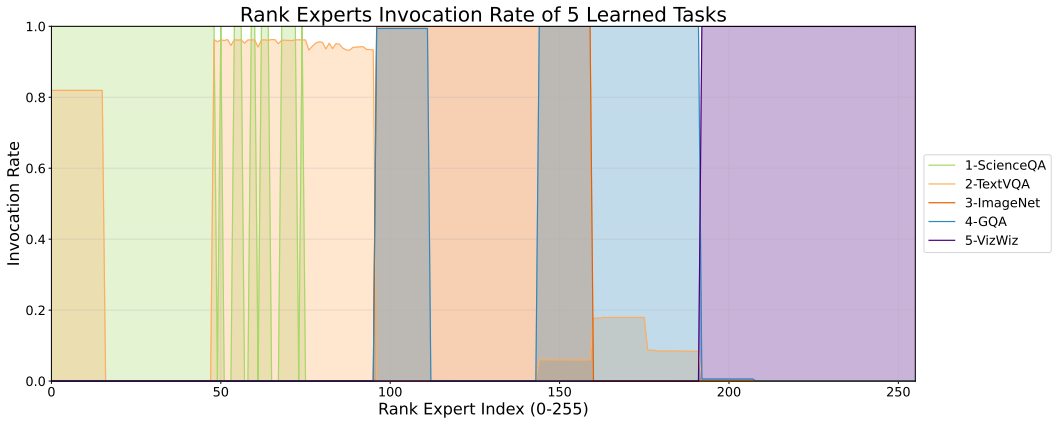

Figure 10: The invocation rate of rank experts after learning the 5-th task VizWiz.

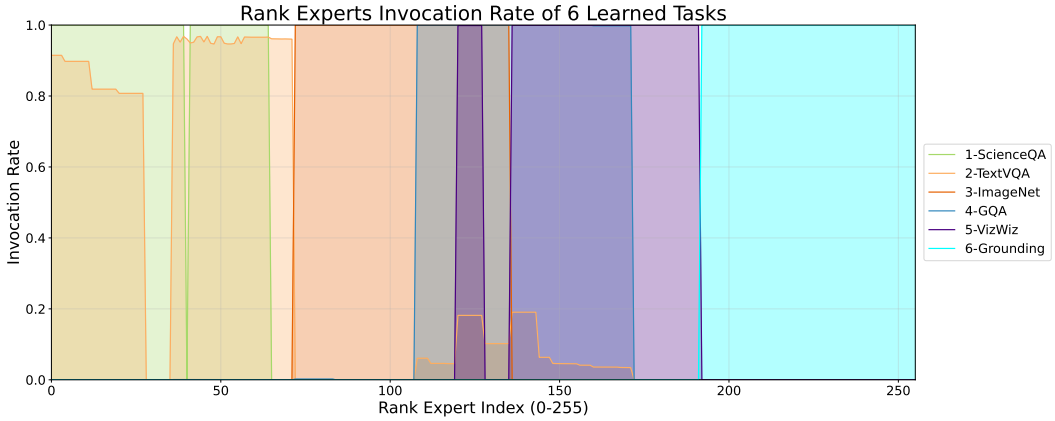

Figure 11: The invocation rate of rank experts after learning the 6-th task Grounding.

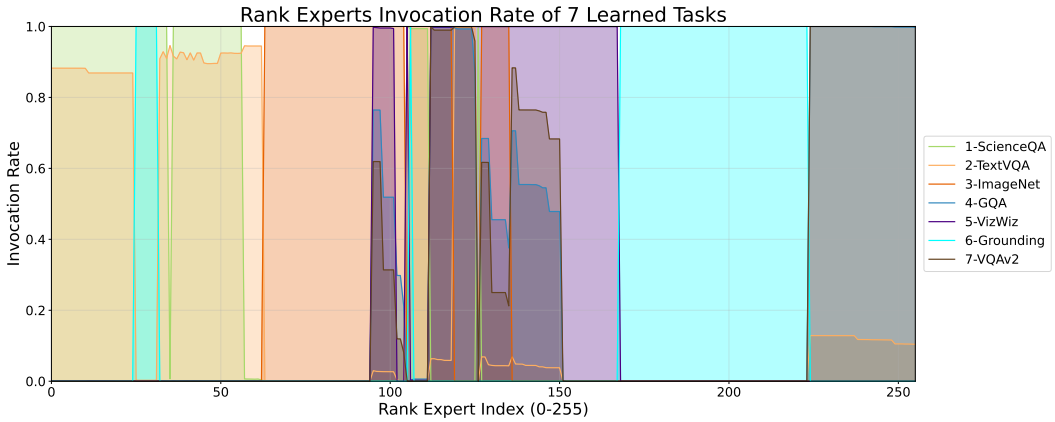

Figure 12: The invocation rate of rank experts after learning the 7-th task VQAv2.

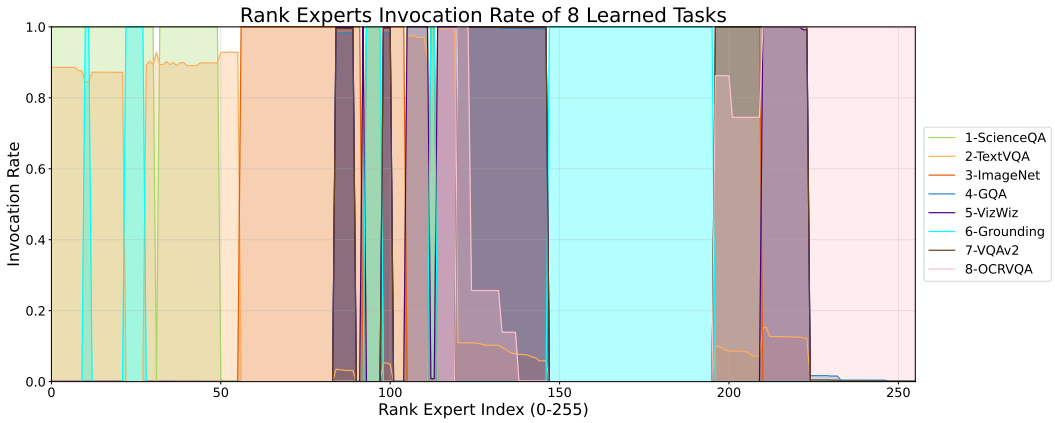

Figure 13: The invocation rate of rank experts after learning the 8-th task OCRVQA.

G THE RESULTS OF CONTINUAL-NEXT BENCHMARK

We present the performance of PCLR and its variant PCLR-LwF on the Continual-NExT benchmark, and we visualize the final accuracies of two representative models (LLaVA-1.5-hf and

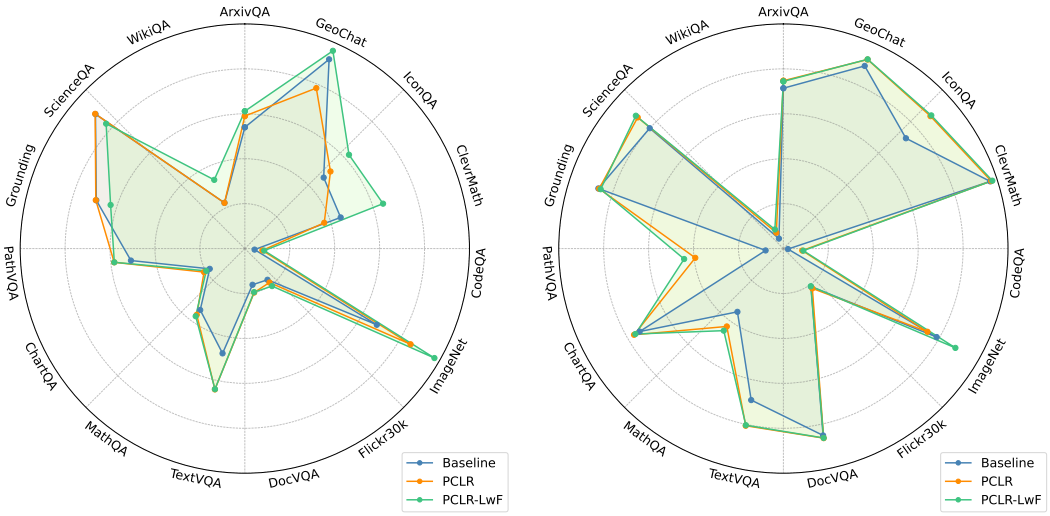

(a) Comparison on LLaVA-1.5-hf

(b) Comparison on Qwen2.5-VL-Instruct

Figure 14: Radar chart of comparisons on Accuracy between baseline (LoRA) and ours.

Qwen2.5-VL-Instruct) using radar charts. As shown in Figure 14, PCLR achieves significant baseline improvements. Notably, PCLR-LwF incorporates LwF (Li & Hoiem, 2017) which is regularized to reduce the compression demand, achieving improved computational efficiency while further improving the performance of PCLR. Thus, PCLR enables compatibility with other continual learning algorithms, offering a practical solution for deployment in real-world applications.

H Three Types of Tuning Order Sequences

To evaluate robustness under different Continual Instruction Tuning orders, we employ three task ordering strategies:

1. **Original Order**: Tasks are presented in the default sequence: ScienceQA, TextVQA, ImageNet, GQA, VizWiz, Grounding, VQAv2, OCRVQA.
2. **Reverse Order**: The sequence is reversed relative to the original: OCRVQA, VQAv2, Grounding, VizWiz, GQA, ImageNet, TextVQA, ScienceQA.
3. **Alphabetical Order**: Tasks are sorted alphabetically: GQA, Grounding, ImageNet, OCRVQA, ScienceQA, TextVQA, VizWiz, VQAv2.

I Three Types of Instruction Templates

To evaluate robustness under different instruction templates, we adopt three types of instruction templates. Detailed examples of these templates are provided in Table 20.

1. **Original Instruction Template**: Each task is associated with a single instruction, and multiple tasks may share identical instruction formats. This setting reflects minimal prompt diversity.
2. **Diverse Instruction Template**: Each task uses a single, uniquely designed instruction. Instructions are carefully tailored to reflect the semantic and structural characteristics of individual tasks, maximizing prompt diversity.
3. **10Type Instruction Template**: Each task is assigned approximately ten distinct instruction variants. While instructions are diverse within each task, certain templates may be shared across related tasks, simulating a balanced scenario between diversity and generalization.

J Detailed Settings for Different Compression Strategies

All settings are maintained at total rank = 256, activated rank = 64, and share rank = 32.

Aggressive: The compression retention rate is fixed at 75%, and the number of new rank experts is fixed at 64.

Conservative: The compression retention rate is fixed at 87.5%, and the number of new rank experts is fixed at 64.

Reverse: The compression retention rate changes from 87.5% $\rightarrow$ 75%, with the number of new rank experts fixed at 32 $\rightarrow$ 64.

Centralized: The first eight tasks are not compressed, and after all tasks are learned, a 50% retention rate compression is applied (forgetting is calculated based on 8 tasks). In terms of integration data, compared to the Ours (integrating on the current dataset after each learning cycle), it is relatively singular (the last integration only shows OCRVQA data).

Ours: The compression retention rate changes from 75% $\rightarrow$ 87.5%, with the number of new rank experts fixed at 64 $\rightarrow$ 32.

The dynamic adjustment strategy we adopt is based on the distillation loss during the integration phase: if, within the 50th–70th training steps of the integration process, at least 25% of the fake queries (i.e., 25% of the learned tasks) exhibit KL divergence losses exceeding a predefined threshold (set to 0.05 in this paper), it is determined that the current compression intensity is too high, causing significant knowledge conflicts between tasks. This occurs because the optimization objectives of different tasks generate severe discrepancies over the same rank components, leading to interference in task-specific information.

In such cases, the system increases the retention rate and re-executes the compression-integration process, reducing the degree of information fusion between tasks to mitigate the loss of historical knowledge. Simultaneously, during the learning phase of subsequent tasks, the number of newly added ranks is correspondingly reduced (e.g., from 64 to 32) to maintain the total parameter capacity constant.

K Task Grouping of PCLR-LwF

Task Grouping for LLaVA-1.5-hf:

Group 1: 1-ArxivQA, 2-GeoChat, 3-IconQA

Group 2: 4-ClevrMath

Group 3: 5-CodeQA, 6-ImageNet

Group 4: 7-Flickr30k, 8-DocVQA, 9-TextVQA

Group 5: 10-MathQA, 11-ChartQA, 12-PathVQA

Group 6: 13-Grounding, 14-ScienceQA, 15-WikiQA

Using a compression retention ratio of 66.67%, the final PCLR consists of 256 expert ranks.

Task Grouping for Qwen2.5-VL-Instruct:

Group 1: 1-ArxivQA, 2-GeoChat, 3-IconQA

Group 2: 4-ClevrMath, 5-CodeQA, 6-ImageNet

Group 3: 7-Flickr30k, 8-DocVQA, 9-TextVQA

Group 4: 10-MathQA, 11-ChartQA, 12-PathVQA

Group 5: 13-Grounding, 14-ScienceQA, 15-WikiQA

Using a compression retention ratio of 80%, the final PCLR consists of 256 expert ranks.

This different grouping strategy is motivated by the observation that the LLaVA-1.5-hf after training on ImageNet performs worse on ClevrMath. To address this, we place the ClevrMath task in a

dedicated group. The memory budget can be mitigated by either reducing the compression retention ratio or increasing the number of compression times.

L Comparison of Training Cost with MoELoRA

Table 12: The Training Cost of LLaVA about **different numbers of experts**.

Number	Training Cost on Each Task (Unit: Minutes)								
	1-ScienceQA	2-TextVQA	3-ImageNet	4-GQA	5-VizWiz	6-Grounding	7-VQAV2	8-OCRVQA	Average
1	10.05	33.55	91.22	118.12	17.78	79.58	93.44	135.68	72.43
2	17.73	50.97	130.61	173.58	27.94	115.71	136.53	188.86	105.24
4	21.25	68.14	189.05	245.97	35.25	169.12	205.52	286.92	152.65
Ours	**8.86**	**34.43**	**94.82**	**115.49**	**19.85**	**93.68**	**121.87**	**177.12**	**83.27**

As discussed in the main paper, all computations in our fine-grained LRP, are fully parallelizable. On LLaVA-13B, we compare LRP (total rank 256, activated rank 64, shared rank 32) with MoELoRA (total and activated rank of 128) variants having 1, 2, and 4 experts, as summarized in Table 12.

The forward computation of MoELoRA is defined as:

$$y = xW + \beta \sum_{i=1}^{t} s(x)_i x A_i B_i^T, \tag{11}$$

where $s(x) \in \mathbb{R}^t$ denotes the expert routing scores, t is the number of total experts, k is the number of activated experts, and A_i, B_i are the LoRA weights of the i-th expert.

The proposed LRP forward computation in the main paper is formulated as:

$$y = xW + \beta_s x A_s B_s^T + \beta_m F\left(xA_m, gate\left(Kq, r\right)^T\right) B_m^T, \tag{12}$$

where A_s, B_s represent the globally shared components, and A_m, B_m represent the mixture expert components. The operator $F\left(U, v\right)$ broadcasts $v \in \mathbb{R}^b$ to match the shape of $U \in \mathbb{R}^{a \times b}$, followed by an element-wise multiplication. Here, $K \in \mathbb{R}^{n \times d}, q \in \mathbb{R}^d$ are the L2-regularized key pool and query, n is the number of total rank experts, r is the number of activated rank experts.

MoELoRA consistently activates all ranks and performs serial summation across experts, whereas LRP avoids serial computation by directly integrating expert scores into the LoRA formulation. Specifically, we set the number of experts to match the LoRA rank to align the expert score dimension with the LoRA rank. This design enables parallel integration of expert scores into the LoRA forward computation. This yields efficiency comparable to MoELoRA with one expert because GPU matrix multiplication is faster than serial multiplication and summation over smaller matrices at the same total rank.

M Inspirations from AdaLoRA and the L2P Series

AdaLoRA (Zhang et al., 2023) converts each LoRA adapter into a SVD-style representation, enabling dynamic rank adjustment under a fixed parameter budget and thereby improving computational allocation efficiency. The L2P series (Wang et al., 2022c;b; Smith et al., 2023b) decomposes conventional prompts or prefixes into subcomponent representations paired with learnable keys. It further introduces a dynamic parameter allocation mechanism, markedly improving performance and efficiency in continual learning for the vision domain (Krizhevsky et al., 2009; Peng et al., 2019).

Inspired by AdaLoRA, we likewise decompose LoRA updates into rank vectors but remove explicit rank constraints, and adopt an L2P-like key–value matching scheme, we associate each rank vector with a learnable key and allow dynamic extension during CIT. This simultaneously (i) extends the L2P series to the more parameter-efficient LoRA paradigm, facilitating adaptation to LMMs, and (ii) generalizes adaptive rank allocation principle of AdaLoRA to a Mixture-of-Experts (MoE) structure tailored for continual learning. In summary, we introduce the LoRA Rank Pool (LRP), an extremely fine-grained MoE architecture that offers maximum flexibility for knowledge employment and editing to enhance stability and plasticity.

N EXPLANATION OF RELATIVE REDUNDANCY RANK

In this section, we provide a detailed definition of the relative redundancy rank, namely the relative redundancy rank of M to N for the LoRA pair $\langle M, N\rangle$. We select an arbitrary identically named weight pairs $\{(A_M, B_M), (A_N, B_N)\}_i$ and perform an orthogonal triangle decomposition on A_N:

$$QR = A_N, \tag{13}$$

where $A_M, A_N \in \mathbb{R}^{d_{in} \times r}$, $Q \in \mathbb{R}^{d_{in} \times r}$, and Q is a set of orthogonal vectors of A_N. Subsequently, we apply L2 normalization to every column of A_M, producing $\widetilde{A_M}$. For each $a \in \mathbb{R}^{d_{in} \times 1}$ in $\widetilde{A_M}$, we use Q to reconstruct:

$$a^* = QQ^T a, \tag{14}$$

Therefore, we can obtain the reconstruction loss for the part $\langle a, A_N\rangle$:

$$\mathcal{L}_a = 1 - \|a^*\|_2^2. \tag{15}$$

$\mathcal{L}_a \in [0, 1]$ reflects the degree of linear dependence between a and the vectors in A_N, a smaller value indicates a higher degree of linear dependence. When $\mathcal{L}_a = 0$, a and A_N are linearly dependent. When $\mathcal{L}_a = 1$, the inner product between a and every $v \in A_N$ is zero.

Similarly, we can obtain the reconstruction loss for the part of $\langle b, B_N\rangle$, $\mathcal{L}_b \in [0, 1]$. Next, we define the reconstruction loss for the rank $(a, b) \in (A_M, B_M)$ with respect to LoRA (A_N, B_N):

$$\mathcal{L} = \mathcal{L}_a * \mathcal{L}_b, \tag{16}$$

$\mathcal{L} \in [0, 1]$ reflects the degree of linear dependence between the rank component $(a, b) \in (A_M, B_M)$ and the LoRA weight pair (A_N, B_N). According to the theoretical insights from LoRA (Hu et al., 2022) and AdaLoRA (Zhang et al., 2023), rank components that are linearly dependent are redundant, and they carry knowledge similar to other rank components, which is the knowledge redundancy referred to in the main text.

We define the threshold $\sigma = 0.001$. For each rank component $(a, b) \in (A_M, B_M)$ relative to the LoRA weight (A_N, B_N), if its score $\mathcal{L} < \sigma$, this component is deemed a redundant rank. Next, we obtain the redundancy rank ratio of (A_M, B_M) relative to (A_N, B_N) (the corresponding LoRA weight pairs $\{(A_M, B_M), (A_N, B_N)\}_i$). Finally, by computing $\mathcal{L}$ of all attention modules, we obtain the relative redundancy rank ratio for $\langle M, N\rangle$ (M relative to N).

O THE EFFECT OF EPOCH ON PCLR

To verify the impact of epoch count on PCLR's performance and forgetting resistance, we conducted experiments on the LLaVA-1.5-7b model and the CoIN benchmark, setting training cycles of 1, 3, and 5 epochs to compare the performance of PCLR and PGP:

Table 13: Results of LLaVA-1.5-7B on **PGP and PCLR methods with different epochs**.

Methods-Epoch	Final Accuracy on Each Task								Overall Results		
	ScienceQA	TextVQA	ImageNet	GQA	VizWiz	Grounding	VQAv2	OCRVQA	Avg.ACC	Forgetting	New.ACC
PGP-1	85.17	56.85	32.26	61.74	49.43	32.74	65.74	62.20	55.77	12.94	67.09
PGP-3	85.38	57.14	32.59	62.15	49.68	33.12	66.06	62.43	56.07	12.76	67.24
PGP-5	85.50	57.43	32.75	62.31	49.88	33.46	66.22	62.67	56.28	12.63	67.33
PCLR-1	78.33	58.24	86.08	58.14	57.61	33.04	64.17	61.92	62.19	3.39	65.16
PCLR-3	84.56	59.73	91.66	57.31	58.12	35.65	65.03	62.06	64.27	2.75	66.68
PCLR-5	86.04	59.24	93.29	55.64	57.81	36.82	64.41	61.69	64.37	2.36	66.43

Note: To ensure fairness, the integration data usage (IDU) for PCLR-1, PCLR-3, and PCLR-5 remains the same.

PGP shows limited improvement over longer epochs: Although PGP restricts updates through gradient constraints, during longer epoch training, the trainable parameters gradually skew toward the optimal solution for the current task, leading to overwriting of historical knowledge and maintaining high forgetting rates (12.94 → 12.76 → 12.63).

PCLR's CIL mechanism demonstrates stronger performance over longer epochs: During training with 3 and 5 epochs, PCLR's forgetting rate remains significantly lower than PGP (2.75 *v.s.* 12.94,

2.36 *v.s.* 12.63), and the Avg.ACC. continues to improve (62.19 → 64.27 → 64.37), the Forgetting continues to reduce (3.39 → 2.75 → 2.36).

We can analyze the reasons for the performance improvement from the perspective of CIL. Learning phase: New tasks only update newly added rank experts, avoiding interference with historical knowledge, so increasing training epochs does not lead to forgetting. Integration phase: A well-learned set of parameters has less noise, and it is easier for compatible representations to emerge across different tasks, which is beneficial for integration. Knowledge distillation merges new and old knowledge, ensuring stability improvement. The time spent in this phase has a positive feedback relationship with the effectiveness of forgetting resistance.

In summary, PCLR's design not only adapts to tasks with varying training lengths but also excels in multi-epoch training, ensuring efficient knowledge integration and low forgetting rates.

P More Ablation Experiments

In this section, we discuss how to balance CIT performance and memory efficiency from two perspectives: knowledge density and memory scale. For more intuitive comparisons, we use **total rank experts + shared ranks** to measure the static storage parameters (SSP) and **activated rank experts + shared ranks** to measure the inference activated parameters (IAP).

Table 14: Results of LLaVA-1.5-7B on **different knowledge density**.

Method	Rank Allocation		Final Accuracy on Each Task								Overall Results		
	SSP	IAP	ScienceQA	TextVQA	ImageNet	GQA	VizWiz	Grounding	VQAv2	OCRVQA	Avg.ACC	Forgetting	New.ACC
Dense Space	192+32	64+32	72.01	53.68	88.32	58.19	55.20	30.82	64.38	63.40	60.75	4.83	64.98
Sparse Space	320+32	64+32	80.71	59.36	90.81	56.82	56.05	31.32	65.13	62.50	62.84	2.65	65.16
Dynamic Space	384+32	64+32	81.54	59.37	93.05	56.44	57.05	30.80	64.46	62.80	63.19	2.06	65.00
Ours	256+32	64+32	78.33	58.24	86.08	58.14	57.61	33.04	64.17	61.92	62.19	3.39	65.16

Dense Space: With total rank experts = 192, the initial compression retention rate is adjusted to 66.67%, and the compression strategy is 66.67% → 88.33%, with new ranks changing from 64 → 32. 1/3 of the experts are activated during inference, resulting in dense knowledge compression and significant overlap among rank experts. Consequently, Avg.ACC decreases (60.75), Forgetting increases (4.83), and SSP reduces by 22.22% compared to ours.

Sparse Space: With total rank experts = 320, the initial compression retention rate is adjusted to 80%, and the compression strategy is 80% → 90%, with new ranks changing from 64 → 32. 1/5 of the experts are activated during inference, with weaker sharing among rank experts. Consequently, Avg.ACC increases (62.84), Forgetting decreases (2.65), and SSP rises by 22.22% compared to ours.

Dynamic Space: Total rank experts dynamically change from 256 → 384, with 32 ranks compressed and 64 ranks added at each step. This setting achieves the highest Avg.ACC (63.19), the lowest Forgetting (2.06), and the largest final SSP.

The data shows that forgetting largely depends on the **knowledge density** of the PCLR parameter space (activated rank experts / total rank experts). Higher values tend to favor knowledge integration, while lower values favor expert specialization. Knowledge density is a flexible parameter designed to balance memory efficiency and continual learning capability. It can be adjusted based on memory constraints (there is no universally optimal setting; it depends on memory conditions).

In summary, the **optimal compression strategy** involves a transition from **aggressive to conservative**, and the **initial compression rate** can be **adjusted as needed**. We do not recommend treating it as a fixed parameter.

Table 15: Results of LLaVA-1.5-7B on **different memory scale**.

Method	Rank Allocation		Final Accuracy on Each Task								Overall Results		
	SSP	IAP	ScienceQA	TextVQA	ImageNet	GQA	VizWiz	Grounding	VQAv2	OCRVQA	Avg.ACC	Forgetting	New.ACC
Small-Scale	128+0	32+0	78.87	58.23	82.16	56.77	53.81	30.76	63.86	60.14	60.58	4.13	64.19
No Shared	256+0	64+0	78.59	58.09	88.57	56.93	55.29	31.96	64.41	62.40	62.03	3.63	65.21
Ours	256+32	64+32	78.33	58.24	86.08	58.14	57.61	33.04	64.17	61.92	62.19	3.39	65.16

Small-Scale Parameter Space: Compared to **No Shared**, memory usage is halved, but performance declines across the board: Avg.ACC (62.03 → 60.58), Forgetting (3.63 → 4.13), and New.ACC (65.21 → 64.19). This reflects insufficient plasticity and severe parameter contention, leading to increased forgetting.

No Shared Ranks: Compared to ours, the lack of shared ranks during integration prevents the absorption of global knowledge, resulting in higher forgetting (3.39 → 3.63).

The data in the table indicates that the scale of the parameters is positively correlated with model performance. **Small-Scale**, despite having the same total parameter space as regularization-based methods, only utilizes 1/4 of the activated/trained parameters, yet it still outperforms PGP (55.77) and SEFE (58.57), which are among the best regularization-based methods. Both **No Shared** and Ours, with fewer activated parameters and a fixed memory budget, surpass the extension-based method Eproj (60.79) in performance.

Q Memory Efficiency Comparison

Using the LLaVA-1.5-7b model on the CoIN benchmark, we further compared PGP, Eproj, PCLR-small (0 shared, 32 active, 128 total), and PCLR-ours (32 shared, 64 active, 256 total), trainable parameters, and final performance (all statistics exclude the base model and focus solely on the adapter components).

Table 16: PGP, parameters and accuracy across tasks.

Metric	Tasks							
	ScienceQA	**TextVQA**	**ImageNet**	**GQA**	**VizWiz**	**Grounding**	**VQAv2**	**OCRVQA**
Total Params	340.80M	340.80M	340.80M	340.80M	340.80M	340.80M	340.80M	340.80M
Activated Params	340.80M	340.80M	340.80M	340.80M	340.80M	340.80M	340.80M	340.80M
Trainable Params	340.80M	340.80M	340.80M	340.80M	340.80M	340.80M	340.80M	340.80M
Final Accuracy	85.17	56.85	32.26	61.74	49.43	32.74	65.74	62.20

Table 17: Eproj, parameters and accuracy across tasks.

Metric	Tasks							
	ScienceQA	**TextVQA**	**ImageNet**	**GQA**	**VizWiz**	**Grounding**	**VQAv2**	**OCRVQA**
Total Params	340.80M	660.61M	980.43M	980.43M	980.43M	1300.24M	1300.24M	1300.24M
Activated Params	340.80M	340.80M	340.80M	340.80M	340.80M	340.80M	340.80M	340.80M
Trainable Params	340.80M	340.80M	340.80M	340.80M	340.80M	340.80M	340.80M	340.80M
Final Accuracy	78.51	57.53	92.35	55.93	44.67	36.59	63.74	57.00

Table 18: PCLR-small, parameters and accuracy across tasks.

Metric	Tasks							
	ScienceQA	**TextVQA**	**ImageNet**	**GQA**	**VizWiz**	**Grounding**	**VQAv2**	**OCRVQA**
Total Params	85.79M	171.58M	257.37M	343.16M	343.16M	343.16M	343.16M	343.16M
Activated Params	85.79M	85.79M	85.79M	85.79M	85.79M	85.79M	85.79M	85.79M
Trainable Params	85.79M	85.79M	85.79M	85.79M	85.79M	85.79M	42.90M	42.90M
Final Accuracy	78.87	58.23	82.16	56.77	53.81	30.76	63.86	60.14

Table 19: PCLR-ours, parameters and accuracy across tasks.

Metric	Tasks							
	ScienceQA	**TextVQA**	**ImageNet**	**GQA**	**VizWiz**	**Grounding**	**VQAv2**	**OCRVQA**
Total Params	171.58M	343.16M	514.74M	686.31M	766.70M	766.70M	766.70M	766.70M
Activated Params	171.58M	171.58M	171.58M	171.58M	251.97M	251.97M	251.97M	251.97M
Trainable Params	171.58M	171.58M	171.58M	171.58M	171.58M	171.58M	85.79M	85.79M
Final Accuracy	78.33	58.24	86.08	58.14	57.61	33.04	64.17	61.92

PCLR imposes a strict upper bound on total ranks, halting parameter growth after early expansion via compression-integration. In contrast, Eproj expands continuously, risking parameter explosion. PCLR outperforms both PGP and Eproj in average accuracy (**62.19** *v.s.* **55.77 / 60.79**) and forgetting (**3.39** *v.s.* **12.94 / 5.42**), demonstrating its ability to control memory while maintaining strong continual learning performance.

When the total parameter count is constrained to a level similar to PGP, PCLR still achieves competitive performance with an Avg.ACC of **60.58**, close to Eproj (**60.79**) and significantly higher than PGP (**55.77**). These results demonstrate that PCLR can effectively utilize limited resources, providing robust performance even under strict parameter budget constraints.

R MODELS

LLaVA-1.5 (Liu et al., 2024): LLaVA-1.5 is a foundational Large Multimodal Model (LMM) that integrates Vicuna (Chiang et al., 2023) as its large language model (LLM) backbone and CLIP-ViT (Radford et al., 2021) as the visual encoder. The cross-modal bridge module employs linear projection layers to align visual features with linguistic representations. Specifically, CLIP-ViT extracts image embeddings, which are then projected through a linear transformation to match the hidden dimension of Vicuna. This design enables efficient fusion of visual and textual information for downstream tasks such as visual question answering (VQA) and image captioning. In this paper, we use LLaVA-1.5-7B[1], LLaVA-1.5-13B[2], and LLaVA-1.5-7B-hf[3] (a fine-tuned version of LLaVA-1.5-7B).

Qwen-VL (Bai et al., 2023b): Qwen-VL[4] is a Visual-Large Language Model (VLLM) developed by Alibaba Cloud, combining QwenLM (Bai et al., 2023a) as its LLM backbone and a Vision Transformer (ViT) for visual encoding. Its cross-modal bridge module utilizes Q-Former (a transformer-based architecture) designed for multi-modal feature fusion. The Q-Former attends to visual and textual tokens, enabling context-aware interaction between modalities.

Qwen2.5-VL (Bai et al., 2025): Qwen2.5-VL is an advanced version of Qwen-VL (Bai et al., 2023b), featuring Qwen2.5-LM (Yang et al., 2025) as its LLM backbone and a cross-modal architecture. Its cross-modal bridge module works as follows: RMSNorm first normalizes the visual features, followed by a three-layer MLP that projects them into the linguistic space. This replaces the Q-Former in Qwen-VL with a lightweight yet powerful structure, enabling more efficient parameter allocation. Qwen2.5-VL-Instruct[5] builds upon Qwen2.5-VL through supervised fine-tuning on curated, high-quality instruction data, improving its adaptability to downstream tasks.

S METHODS

LoRA (Base) (Hu et al., 2022): LoRA is a parameter-efficient fine-tuning method that introduces low-rank decomposition matrices into the weight matrices of pretrained models. By freezing the original model weights and using low-rank matrices to capture task-specific information, LoRA significantly reduces the number of trainable parameters while preserving the model's generalization ability. It is widely applied in natural language processing and computer vision due to its low memory consumption, fast training speed, and support for multi-task adaptability.

MoELoRA (Chen et al., 2024a): MoELoRA combines the Mixture-of-Experts (MoE) mechanism with Low-Rank Adaptation (LoRA) to enhance adaptability in dynamic task environments. It dynamically allocates expert resources and adjusts modality-specific adaptation weights, achieving improved multi-task performance. In our CIT setting, the number of experts is set to 2 per MoE layer. It is static-structure-based.

Learning Without Forgetting (LwF) (Li & Hoiem, 2017): LwF addresses catastrophic forgetting through knowledge distillation. A pretrained model guides the current model to retain historical task knowledge without requiring access to old datasets. It enforces alignment between the output distribution of the current model and the teacher model by combining next-token prediction loss and distillation loss with a weighted sum of two losses of two losses. It is regularization-based.

Elastic Weight Consolidation (EWC) (Kirkpatrick et al., 2017): EWC introduces a regularization term based on the Fisher Information Matrix (FIM) to protect critical parameters from previous tasks. By computing parameter importance (diagonal elements of FIM) and imposing constraints during new task training, EWC balances old and new task performance. It is regularization-based.

Gradient Episodic Memory (GEM) (Lopez-Paz & Ranzato, 2017): GEM prevents forgetting by maintaining episodic memory of historical task samples and enforcing gradient constraints. It projects the current task gradient into a subspace compatible with all historical gradients via

[1] https://huggingface.co/liuhaotian/llava-v1.5-7b

[2] https://huggingface.co/liuhaotian/llava-v1.5-13b

[3] https://huggingface.co/llava-hf/llava-1.5-7b-hf

[4] https://huggingface.co/Qwen/Qwen-VL

[5] https://huggingface.co/Qwen/Qwen2.5-VL-3B-Instruct

quadratic programming, ensuring new task updates do not degrade old task performance. It is regularization-based and replay-based. We set 100 samples per task for replay.

Experience Replay (Rolnick et al., 2019): Experience Replay mitigates catastrophic forgetting by replaying subsets of historical data during new task training. A replay buffer stores representative samples, and the model alternates between learning new data and reinforcing old knowledge through mixed training. It is replay-based. We set 100 samples per task for replay.

Prompt Gradient Projection (PGP) (Qiao et al., 2025b): PGP proposes a gradient projection approach that enforces model parameter updates to be orthogonal to the previous feature subspace, thereby preserving historical knowledge and enabling adaptation to new tasks. It is regularization-based.

Model Tailor (MT) (Zhu et al., 2024): MT restricts training to the critical parameters while compensating for variations in the trainable parameters. It is regularization-based.

Eproj (He et al., 2023): Eproj is an advanced dynamic model adaptation method. It groups high-conflict tasks and handles low-conflict tasks via regularization. It is extension-based.

Dynamic EMA (CIA*) (Qiao et al., 2025a): CIA* derives optimal balance weights from the trade-off premise and EMA update, satisfying plasticity-stability conditions. The weights are adaptively determined by gradients and learned parameters. It is regularization-based.

Dynamic EMA + Instruction Grouping (CIA) (Qiao et al., 2025a): CIA extends CIA* by introducing instruction grouping to avoid high-conflict tasks. Based on instruction semantic similarity, it determines whether to retrain or extend parameters and allocates the most suitable parameters for testing instances. It is extension-based.

PCLR (Ours): PCLR introduces two key innovations to address the challenges of continual instruction tuning (CIT) in Large Multimodal Models (LMMs). First, we decompose LoRA weights into LoRA Rank Pool (LRP), enabling fine-grained control over expert ranks and achieving flexible parameter allocation. This design supports arbitrary compression ratios while preserving task-specific adaptability. Then, we propose the Compression-Integration-Learning (CIL) pipeline, which balances plasticity and stability through three stages:

(1) Compression: It prunes rank experts to reserve space for new task learning.

(2) Integration: It fuses knowledge from similar experts via distillation to enhance synergy.

(3) Learning: It trains new experts in the released space without memory explosion.

PCLR-LwF (A Simplified Variant of PCLR) To further enhance the performance of PCLR on long-term CIT while minimizing unnecessary performance degradation and training overhead, we propose PCLR-LwF, a simplified variant that combines PCLR with LwF (Li & Hoiem, 2017). We group consecutive tasks into clusters, we apply LwF within each cluster for continual instruction tuning. This approach preserves the core advantages of PCLR and significantly reducing the cost of integration.

T DATASETS

ScienceQA (Lu et al., 2022): ScienceQA is a multimodal science question-answering dataset designed to evaluate the ability of models to perform reasoning by integrating visual and textual information. The training dataset comprises 12,726 samples, with 6,218 instances in the image-text modality and 6,508 in the text-only modality. The testing dataset contains 4,241 samples, distributed as 2,017 image-text instances and 2,224 text-only instances.

TextVQA (Singh et al., 2019): TextVQA targets text recognition in visual question-answering. The dataset includes real-world images with diverse text formats (handwritten, printed). The training dataset comprises 34,602 samples, all of which belong to the image-text modality. The testing dataset contains 5,000 samples, all of which are in the image-text modality.

ImageNet (Russakovsky et al., 2015): ImageNet is a large-scale image classification dataset. The training dataset comprises 129,833 samples, all of which belong to the image-text modality. The testing dataset contains 5,050 samples, all of which are in the image-text modality.

GQA (Hudson & Manning, 2019): GQA emphasizes real-world visual reasoning. It evaluates understanding of object relationships and perform multi-step inference. The dataset includes both synthetic and real-world images with scene graphs for structured reasoning. The training dataset comprises 72,140 samples, all of which belong to the image-text modality. The testing dataset contains 12,578 samples, all of which are in the image-text modality.

VizWiz (Gurari et al., 2018): VizWiz is a visual question-answering dataset for visually impaired users. The dataset focuses on practical, everyday visual queries. The training dataset comprises 20,523 samples, all of which belong to the image-text modality. The testing dataset contains 4,319 samples, all of which are in the image-text modality.

Grounding (Mao et al., 2016): The Grounding tests the ability of models to align natural language instructions with objects in images. It includes image-text pairs where the text describes object locations or attributes, and the task is to predict the corresponding bounding boxes. The training dataset comprises 55,885 samples, all of which belong to the image-text modality. The testing dataset contains 30,969 samples, all of which are in the image-text modality.

VQAv2 (Goyal et al., 2017): VQAv2 is a foundational visual question-answering dataset. It emphasizes balanced answer distributions and diverse topics. The training dataset comprises 82,783 samples, all of which belong to the image-text modality. The testing dataset contains 214,354 samples, all of which are in the image-text modality.

OCRVQA (Mishra et al., 2019): OCRVQA combines optical character recognition with visual question-answering. It evaluates models' ability to parse text from images and generate answers based on the extracted content. The training dataset comprises 165,348 samples, all of which belong to the image-text modality. The testing dataset contains 99,926 samples, all of which are in the image-text modality.

ArXivQA (Li et al., 2024b): ArXivQA is a multi-modal dataset for scientific paper analysis. It includes images, formulas, and text from arXiv papers, with questions requiring cross-modal reasoning for tasks such as figure interpretation or explaining derivations. The training dataset comprises 90,000 samples, all of which belong to the image-text modality. The testing dataset contains 10,000 samples, all of which are in the image-text modality.

GeoChat (Kuckreja et al., 2024): GeoChat focuses on geospatial reasoning using maps. It includes map images and natural language questions about locations, terrain features, or symbols. The training dataset comprises 25,362 samples, all of which belong to the image-text modality. The testing dataset contains 3,000 samples, all of which are in the image-text modality.

IconQA (Lu et al., 2021): IconQA targets abstract icon understanding. It contains icon-text pairs where models must match icons to their descriptions, testing semantic parsing of symbolic visual elements. The training dataset comprises 29,859 samples, all of which belong to the image-text modality. The testing dataset contains 3,000 samples, all of which in the image-text modality.

ClevrMath (Lindström & Abraham, 2022): ClevrMath includes synthetic images and math problems (geometry, arithmetic) and requires models to perform compositional logic and computation. The training dataset comprises 40,000 samples, all of which belong to the image-text modality. The testing dataset contains 3,000 samples, all of which are in the image-text modality.

CodeQA (Liu & Wan, 2021): CodeQA is a programming question-answering dataset. It pairs code snippets with questions, testing the ability of models to understand and explain code logic across multiple programming languages. The training dataset comprises 150,896 samples, all of which belong to the text-only modality. The testing dataset contains 18,997 samples, all of which in the text-only modality.

Flickr30k (Plummer et al., 2015): Flickr30k is an image captioning dataset. It supports fine-grained visual-linguistic alignment tasks. The training dataset comprises 30,000 samples, all of which belong to the image-text modality. The testing dataset contains 1,783 samples, all of which are in the image-text modality.

DocVQA (Mathew et al., 2021): DocVQA focuses on document understanding. It includes scanned documents with questions that require text localization and semantic interpretation in complex layouts. The training dataset comprises 39,463 samples, all of which belong to the image-text modality. The testing dataset contains 5,349 samples, all of which are in the image-text modality.

MathQA (Amini et al., 2019): MathQA is a mathematical problem solving dataset with text-based questions. It emphasizes interpretability and logical reasoning for algebraic and geometric problems. The training dataset comprises 29,837 samples, all of which belong to the text-only modality. The testing dataset contains 2,985 samples, all of which are in the text-only modality.

ChartQA (Masry et al., 2022): ChartQA evaluates quantitative reasoning on charts. Questions involve trend analysis and numerical comparisons. The training dataset comprises 28,299 samples, all of which belong to the image-text modality. The testing dataset contains 2,500 samples, all of which are in the image-text modality.

PathVQA (He et al., 2020): PathVQA is a medical pathology dataset. It focuses on disease identification and cellular structure analysis for clinical applications. The training dataset comprises 19,654 samples, all of which belong to the image-text modality. The testing dataset contains 6,719 samples, all of which are in the image-text modality.

WikiQA (Yang et al., 2015): WikiQA is an open-domain question-answering dataset with question-answer pairs from Wikipedia. The training dataset comprises 20,360 samples, all of which belong to the text-only modality. The testing dataset contains 633 samples, all of which are in the text-only modality.

Table 20: The list of instructions for each task.

Task	Original	Diverse	10Type
ScienceQA	Answer with the option's letter from the given choices directly.	Answer with the option's letter from the given choices directly.	Answer with the option's letter from the given choices directly. Select the correct answer from the given choices and respond with the letter of the chosen option. Determine the correct option from the provided choices and reply with its corresponding letter. Pick the correct answer from the listed options and provide the letter of the selected option. Identify the correct choice from the options below and respond with the letter of the correct option. From the given choices, choose the correct answer and respond with the letter of that choice. Choose the right answer from the options and respond with its letter. Select the correct answer from the provided options and reply with the letter associated with it. From the given choices, select the correct answer and reply with the letter of the chosen option. Identify the correct option from the choices provided and respond with the letter of the correct option. From the given choices, pick the correct answer and respond by indicating the letter of the correct option.
TextVQA	Answer the question using a single word or phrase.	Capture the essence of your response in a single word or a concise phrase.	Answer the question with just one word or a brief phrase. Use one word or a concise phrase to respond to the question. Answer using only one word or a short, descriptive phrase. Provide your answer in the form of a single word or a brief phrase. Use a single word or a short phrase to respond to the question. Summarize your response in one word or a concise phrase. Respond to the question using a single word or a brief phrase. Provide your answer in one word or a short, descriptive phrase. Answer the question with a single word or a brief, descriptive phrase. Capture the essence of your response in one word or a short phrase. Capture the essence of your response in a single word or a concise phrase.
ImageNet	Give the object in the image in the form of a single word or a concise phrase.	Express the object in the image in a single word or a short, descriptive phrase.	Summarize the object in the image in a single word or a brief phrase. Provide the object in the image using a single word or a brief phrase. Give the object in the image in the form of a single word or a concise phrase. Express the object in the image with one word or a short, descriptive phrase. Identify the type of content in the image using one word or a concise phrase. Respond to the object in the image with a single word or a short, descriptive phrase. Describe the content of the image using one word or a concise phrase. Express the object in the image in a single word or a short, descriptive phrase. Use a single word or a short phrase to categorize the image content. Classify the image content using only one word or a brief phrase. Use one word or a short phrase to classify the content of the image.
GQA	Answer the question using a single word or phrase.	Respond to the question briefly, using only one word or a phrase.	Respond to the question with a single word or a short phrase. Respond to the question using only one word or a concise phrase. Answer the question with a single word or a brief phrase. Respond with one word or a short phrase. Provide your answer in the form of a single word or a concise phrase. Respond to the question with just one word or a brief phrase. Answer the question using a single word or a concise phrase. Provide your response using only one word or a short phrase. Respond to the question with a single word or a brief phrase. Respond to the question using just one word or a concise phrase. Answer the question with one word or a short phrase.
VizWiz	Answer the question using a single word or phrase.	Provide a succinct response with a single word or phrase.	Answer the question using only one word or a concise phrase. Respond to the question using only one word or a concise phrase. Respond to the question with a single word or a brief phrase. Provide your answer using just one word or a short phrase. Respond with one word or a concise phrase. Answer the question with just one word or a brief phrase. Use a single word or a short phrase to answer the question. Provide your answer in the form of one word or a brief phrase. Reply to the question using one word or a concise phrase. Answer with a single word or a short phrase. Use one word or a brief phrase to answer the question.
Grounding	Please provide the bounding box coordinate of the region this sentence describes.	Please provide the bounding box coordinate of the region this sentence describes.	Identify and provide the bounding box coordinates that match the description given in this sentence. Extract and provide the bounding box coordinates based on the region described in the sentence. Please provide the bounding box coordinate of the region this sentence describes. Find and provide the bounding box coordinates for the region mentioned in the sentence. Provide the coordinates of the bounding box that correspond to the region described in the sentence. Give the bounding box coordinates as described in the sentence. Determine and provide the bounding box coordinates based on the description in the sentence. Identify and provide the coordinates of the bounding box described in the sentence. Provide the coordinates for the bounding box based on the region described in the sentence. Extract and provide the coordinates for the bounding box described in the sentence. Identify and give the coordinates of the bounding box as described by the sentence.
VQAv2	Answer the question using a single word or phrase.	Answer the question using a single word or phrase.	Answer the question using a single word or phrase. Answer the question with a single word or a brief phrase. Use one word or a short phrase to respond to the question. Answer the question using just one word or a concise phrase. Provide your answer to the question using only one word or a brief phrase. Use a single word or phrase to answer the question. Provide an answer using only one word or a brief phrase. Answer the question succinctly with one word or a brief phrase. Answer the question with just one word or a short phrase. Respond to the question using a single word or a concise phrase.
OCRVQA	Answer the question using a single word or phrase.	Condense your answer for each question into a single word or concise phrase.	Respond to the question with a single word or a short phrase. Answer the question using a single word or a concise phrase. Provide your response using only one word or a short phrase. Use one word or a brief phrase to answer the question. Reply to the question using one word or a concise phrase. Use a single word or a short phrase to answer the question. Use a single word or phrase to answer the question. Provide an answer using only one word or a brief phrase. Provide your answer to the question using only one word or a brief phrase. Respond to the question using a single word or a concise phrase. Answer the question using a single word or phrase.

U ALGORITHM

Algorithm 1: PCLR

Input: Pretrained LMM F, number of task N, training set $\{\{x_i^t, y_i^t\}_{i=1}^{n_t}\}_{t=1}^{T}$, learning rate η_1, η_2, learning loss function $\mathcal{L}_1$, integration loss function $\mathcal{L}_2$, progressive compression retention ratio function α, preset total rank number r_m.
Output: LRP module M.
Initialize: LRP module $M = \varnothing$, fake query pool $T_K = \varnothing$.
for $t = 1, ..., N$ **do**
  1. $M = \mathrm{L}(F, \{x_i^t, y_i^t\}_{i=1}^{n_t}, M, \eta_1, \mathcal{L}_1)$. # Learning (L).
  2. Collect all trained keys and calculate their mean q_k.
  3. $T_K = T_K \cup \{q_k\}$.
  if $rank(M) \geq r_m$ **then**
    $M = \mathrm{CI}(F, \{x_i^t, y_i^t\}_{i=1}^{n_t}, T_K, M, \alpha(t), \eta_2, \mathcal{L}_2)$. # Compression and Integration (CI).
  end
end

Algorithm 2: Learning (L)

Input: Pretrained LMM F, current task dataset D, LRP module M_{old}, learning rate η_1, learning loss function $\mathcal{L}_1$ according to Eq.(4).
Output: LRP module M.
Initialize: M_{new}.
if $M_{old} \neq \varnothing$ **then**
  1. Sample a subset from D and calculate their average query q.
  2. Compute the cosine similarity scores between the keys in M_{old} and the query q, select the top-r indices based on the scores (where r represents the rank of M_{new}), and M_{new} is set to the value of the corresponding vector set.
end
Extend rank space $M = cat[M_{old}, M_{new}]$, freeze the old part, and activate the new part.
for $epoch = 1$ **do**
  for $t = 1, ..., T$ **do**
    1. Draw a mini-batch $B = \{x_i^t, y_i^t\}_{i=1}^{b}$.
    2. Calculate $l = \mathcal{L}_1(F, M, B)$.
    3. Using l to backward.
    4. Update M with learning rate η_1.
  end
end

Algorithm 3: Compression and Integration (CI)

Input: Pretrained LMM F, visible datasets D, task key pool K, original LRP M, retention ratio α, learning rate η_2, integration loss function $\mathcal{L}_2$ according to Eq.(5).
Output: post-integration LRP $\widetilde{M}$.
Initialize: Load K as fake query pool, initialize probability table P of fake query, freeze F and M, using α to get post-compression M to initialize $\widetilde{M}$.
for $epoch = 1$ **do**
  for $t = 1, ..., T$ **do**
    1. Draw a mini-batch $B = \{x_i^t, y_i^t\}_{i=1}^{b}$.
    2. Sample q from K with probability table P.
    3. Calculate integration Loss $l = \mathcal{L}_2(F, M, \widetilde{M}, B, q)$.
    4. Using l to update P by Eq.(6).
    5. Using l to backward.
    6. Update $\widetilde{M}$ with learning rate η_2.
  end
end

Algorithm 4: PCLR-LwF

Input: Pretrained LMM F, number of task N, training set $\{\{x_i^t, y_i^t\}_{i=1}^{n_t}\}_{t=1}^{T}$, learning rate η_1, η_2, learning loss function $\mathcal{L}_1$, integration loss function $\mathcal{L}_2$, progressive compression retention ratio function α, preset total rank number r_m, LwF weight β, Conflict detection function E.
Output: LRP module M.
Initialize: LRP module $M = \varnothing$, fake query pool $T_K = \varnothing$, $n = 0$.
for $t = 1, ..., N$ **do**
  if $E(F, M)$ **then**
    1. $M = \mathrm{L}(F, \{x_i^t, y_i^t\}_{i=1}^{n_t}, M, \eta_1, \mathcal{L}_1)$. # Learning (L).
    2. $n = 0$.
  end
  else
    1. $M = \mathrm{L}_{\mathrm{LwF}}(F, \{x_i^t, y_i^t\}_{i=1}^{n_t}, M, \eta_1, \mathcal{L}_1, n, \beta)$. # Learning with LwF ($\mathrm{L}_{\mathrm{LwF}}$).
    2. $n = n + 1$.
  end
  1. Collect all trained keys and calculate their mean q_k.
  2. $T_K = T_K \cup \{q_k\}$.
  if $M \geq r_m$ **then**
    $M = \mathrm{CI}(F, \{x_i^t, y_i^t\}_{i=1}^{n_t}, T_K, M, \alpha(t), \eta_2, \mathcal{L}_2)$. # Compression and Integration (CI).
  end
end

Algorithm 5: Learning ($\mathrm{L}_{\mathrm{LwF}}$)

Input: Pretrained LMM F, current task dataset D, LRP module M, learning rate η_1, learning loss function $\mathcal{L}_1$ according to Eq.(4), continual LwF number n, LwF weight β.
Output: LRP module M.
Initialize: Copy M as M_{old}, and freeze it, set KLD Loss $\mathcal{L}_{KL}$, L2 regularization function l_2.
for $epoch = 1$ **do**
  for $t = 1, ..., T$ **do**
    1. Draw a mini-batch $B = \{x_i^t, y_i^t\}_{i=1}^{b}$.
    2. Calculate $l = \mathcal{L}_1(F, M, B) + \beta \mathcal{L}_{KL}(F, M, M_{old}, B)$.
    3. Using l to backward.
    4. Update M with learning rate η_1.
  end
end
1. Take out all the keys K_{old} of M_{old} and all the keys K of M.
2. For all $(k_{old,i}, k_i) \in (K_{old}, K)$, $k_i = l_2(n * k_{old,i} + k_i)$.
3. Assign all $k_i \in K$ back.